UNIVERSITAT POLITÈCNICA DE CATALUNYA
BARCELONATECH
Escola d'Enginyeria de Telecomunicació
i Aeroespacial de Castelldefels

TREBALL DE FI DE GRAU

TFG TITLE: Trajectory optimization for noise abatement arrival procedures. Case study at Barcelona airport.

DEGREE: Grau en Enginyeria d'Aeronavegació

AUTHOR: Lluís Palma García

ADVISORS: Xavier Prats
Ramon Dalmau

DATE: July 6, 2018

Títol: Optimització de trajectòries per a procediments d'arribada amb reducció de soroll. Cas pràctic a l'aeroport de Barcelona.

Autor: Lluís Palma García

Directors: Xavier Prats
Ramon Dalmau

Data: 6 de juliol de 2018

Resum

L'objectiu principal d'aquest Treball de Fi de Grau és la implementació d'un optimitzador de trajectòries, basat en la minimització d'una funció objectiu concreta, que descriu l'impacte acústic sobre un conjunt de zones sensibles al soroll.

Per assolir amb èxit l'objectiu desitjat, es defineix un model de soroll convenient on els nivells de soroll percebuts es calculen en funció de la trajectòria de l'avió (altitud, velocitat, empenta, etc.). L'optimitzador utilitzat, desenvolupat per investigadors de la UPC, abans d'aquest treball només permetia optimitzar trajectòries verticals (altitud i velocitat) donada una ruta lateral fixa, per això, ha estat actualitzat, modificant el model dinàmic implementat, per permetre l'optimització en el domini lateral.

A més, amb l'objectiu d'obtenir solucions factibles que compleixin els requisits imposats pels sistemes actuals de gestió del trànsit aeri, s'imposen de forma precisa un conjunt de restriccions operatives. D'aquesta manera, el problema d'optimització es formula com un problema de control òptim, el qual es converteix en un problema de programació no lineal mitjançant mètodes de col·locació directa.

Com a principal aportació d'aquest TFG, es proven les funcions d'interpolació amb splines amb l'objectiu de modelar la graella de mesura que defineix les zones sensibles al soroll. En fer això, s'exposa un nou enfocament no convencional amb la intenció de proposar una metodologia alternativa diferent dels mètodes ben establerts basats en l'aplicació de quadres de punts discrets, oferint, d'aquesta manera, una forma més senzilla de mesurar l'impacte acústic, de manera contínua a través de tota la trajectòria de l'avió.

Finalment, amb l'objectiu d'avaluar el rendiment de l'optimitzador, es presenten dos casos per als quals s'obtenen diferents trajectòries que descendeixen des del nivell de creuer fins a la intercepció, a tres altituds diferents (1000, 2000 i 3.000 ft), del sistema de desembarcament d'instruments. Tots els resultats estan convenientment exposats amb l'objectiu d'obtenir conclusions rellevants. A més, es calculen petjades de soroll amb l'objectiu d'oferir una millor visualització dels resultats.

Com demostren els resultats, la metodologia implementada, on les splines defineixen les diferents àrees sensibles al soroll com una funció contínua i diferenciable, ha demostrat ser més que un mètode eficaç, donant resultats positius en els dos casos exposats.

Title : Trajectory optimization for noise abatement arrival procedures. Case study at Barcelona airport.

Author: Lluís Palma García

Advisors: Xavier Prats
Ramon Dalmau

Date: July 6, 2018

Overview

The main objective of the presented bachelor thesis is the implementation of a trajectory optimizer, based on the minimization of a specific objective function, which describes the noise impact over a set of noise sensitive areas.
In order to successfully achieve the desired goal, a convenient noise model is defined where the perceived noise levels are computed as a function of the aircraft trajectory (altitude, speed, thrust, etc.). In addition, the current in-house trajectory optimizer developed by UPC researchers, which before this work only allowed the optimization of the vertical profile (altitude and speed) given a fixed lateral route, has been improved to allow the optimization in the lateral domain by modifying the model describing the aircraft dynamics. Furthermore, with the purpose of obtaining feasible solutions fulfilling the requirements imposed by current air traffic management systems, a set of operational constraints are accurately imposed. Thus, the optimization problem is formulated as an optimal control problem, which is also converted into a non-linear programming problem by means of direct collocation methods.
As main contribution of this work, splines interpolation functions are tested with the aim of modeling the measurement grid defining the noise sensitive areas. By doing this, a new unconventional approach is exposed with the intention of proposing an alternative methodology distinct from well-established methods based in implementing discrete points grids, offering then, a simpler way of measuring the noise impact, continuously, through the whole aircraft trajectory.
Finally, with the aim of testing the performance of the optimizer, two cases are presented for which different descent trajectories are optimized from the cruise level to the interception of the instrument landing system at three different altitudes (1000, 2000 and 3000 ft). All the results are conveniently exposed with the purpose of obtaining relevant strong evidence-based conclusions. Furthermore, noise footprints are computed with the objective of providing a better visualization of the results.
As the results show, the implemented methodology, where splines define the different noise sensitive areas as a continuous, differentiable function, has proven to be more than an effective method, giving very promising results on the two cases exposed.

Al meu avi

CONTENTS

LIST OF FIGURES

LIST OF TABLES

ACRONYMS AND ABBREVIATIONS

ANP Aircraft Noise and Performance

APM Air Performance Model

ATM Air Traffic Management

BADA Base of Aircraft Data

CAS Calibrated Airspeed

CDA Continous Descent Approach

D3 Demographic Distribution Database

DTED Digital Terrain Elevation Database

ECAC European Civil Aviation Conference

FAA Federal Aviation Agency

FAP Final Approach Point

FL Flight Level

GAMS General Algebraic Modelling System

ICAO International Civil Aviation Organization

ILS Instrument Landing System

INM Integrated Noise Model

ISA International Standard Atmosphere

ISO International Organisation for Standardisation

LAMAX A-weighted Maximum Sound Level

LDLP Low Drag Low Power

MMO Maximum Operating Mach

NADP Noise Abatement Departure Procedures

NAP Noise Abatement Procedure

NLP Non-Linear Programming

NPD Noise-Power-Distance

NSA Noise Sensitive Area

OCP Optimal Control Problem

RF Radius to Fix

RNAV Area Navigation

RWY Runway

SID Standard Instrument Departure Route

STAR Standard Arrival Route

TAS True Airspeed

VMO Maximum Operating Speed

NOMENCLATURE

D aerodynamic drag force

J_i i-th objective optimization function

J_i^* optimal cost value of i-th objective optimization function

L aerodynamic lift force

$L_{max,i}^{NPD}$ L_{max} at the i-th location from the NPD table

$L_{max,i}$ L_{max} at the i-th location

L_{max} A-weighted maximum sound level

L_{max}^* A-weighted maximum sound level threshold

M mach number

N sound pressure level

NI noise index

NSA_j j-th NSA

NSA_s total number of NSAs

N_i^l noise level correction term at the i-th location

N_i sound pressure level at the i-th location

P power setting

T total net thrust force

T_{idle} total net thrust force at idle configuration

W_e eastward local wind component

W_h vertical local wind component

W_n northward local wind component

Δ_I engine installation correction term

Γ lateral distance correction term

Λ lateral attenuation correction term

β elevation angle

χ aerodynamic heading angle

γ aerodynamic flight path angle

μ aerodynamic bank angle

$\vec{\eta}$ event constraints vector

$\vec{\eta}_L$ lower bounds for the event constraints vector

$\vec{\eta}_U$ upper bounds for the event constraints vector

$\vec{\psi}$ path constraints vector

$\vec{\psi}_L$ lower bounds for the path constraints vector

$\vec{\psi}_U$ upper bounds for the path constraints vector

$\vec{u}$ control vector

$\vec{x}$ state vector

$\vec{x}_L$ lower bounds for the state vector

$\vec{x}_U$ upper bounds for the state vector

$\vec{z}$ decision variables vector

ζ long-air-to-ground attenuation

d slant distance

d_i slant distance at the i-th location

e eastward position coordinate

g gravity acceleration constant

h height between the aircraft and the observer

h_p aircraft pressure altitude

l lateral distance between the aircraft and the observer

$l_{NSA}^{(p)}$ set of l distances to the closest NSA for every grid point p

l_{NSA} shortest l value to the closest NSA

$l_{p,j}$ shortest l distance from the grid point p to the j-th NSA

m aircraft mass

n northward position coordinate

n_j number of optimization objectives

n_u number of control variables

n_x number of state variables

n_z vertical load factor

t time

t_0 initial time

t_f final time

v true airspeed

INTRODUCTION

With the increasing trend in the number of aircraft flights, which have increased by 80% between 1990 and 2014, and are forecast to grow by a 45% between 2014 and 2035, the number of people exposed to considerable aircraft noise levels has drastically increased. About 2.5 million people were exposed to noise at 45 major European airports in 2014, and this is expected to grow by a 45% between 2014 and 2035 [1]. Thus, it becomes more clear the importance of finding optimal flight procedures that minimize the impact of the aforementioned increasing acoustic contamination.

In this context, several studies have been conducted aiming to find the best methodology to optimize Noise Abatement Procedures (NAPs). The vast majority of exposed methods [2, 3, 4], place a grid of discrete points covering a different set of locations, where the perceived noise generated by a given aircraft trajectory is measured. Then, a cost function based on the combination of those measurements is minimized by an optimization algorithm. Later, others studies [5], included, Noise Sensitive Areas (NSAs), which were defined by a set of points drawing the borders delimiting each NSA.

This being said, the submitted Final-Bachelor Thesis aims at implementing an optimization of noise abatement procedures, based on the minimization of the noise impact produced over a set of NSAs. Although this time, state-of-the-art methods based on discrete measuring points will be replaced by continuous and differentiable functions, suitable for gradient-based optimization algorithms, defined by means of splines.

In order to successfully achieve the desired goal, DYNAMO (DYNAMic Optimizer) [6], a trajectory optimization framework developed at the ICARUS research team from the Technical University of Catalonia, will be implemented. DYNAMO is capable of computing 4D trajectories in different contexts, offering great flexibility regarding the implementation of different flight profiles and scenarios. However, this framework is specially conceived for computing optimal trajectories in the vertical plane, minimizing different parameters, such as fuel, time, route charges, or a combination thereof, given a fixed lateral route.

For this reason, with the aim of tailoring the software to the project needs, two main contributions will be made. First, the dynamics block, will be expanded in order to enable the optimization of aircraft trajectories not only on the vertical plane but also in the lateral one. Secondly, a noise model will be added with the purpose of optimizing trajectories where noise is set as the objective criteria to be minimized.

Finally, in order to properly proof the concept,a noise abatement procedure for the runway 07L arrival route of the Barcelona-El Prat airport will be generated as a case of study.

CHAPTER 1. BACKGROUND

In order to fully understand the presented strategy for minimizing the noise emitted by aircraft trajectories, an introduction on the basic principles of noise and its effects on humans must be given. Thus, the chapter herein describes the basic physics principle describing noise propagation and its main cause and effect relationships. Also, a concise state of the art on Noise abatement procedures, current implementations and optimization research is given in order to better understand the methodology embraced in this project.

1.1. Noise Modeling

In order to properly understand the state of the art on noise modeling, it is important to state the difference between sound and noise. Sound refers to the physical description of Energy being transmitted through the air (or any other medium) by a longitudinal wave which is sensed by the ear. The ear perceives changes in air pressures reaching the human eardrum; so the greater the difference between pressures, the louder the sound perceived would be. As there is a wide range of different pressures, sound is often expressed by using a logarithmic scale:

$$N = 20\log_{10}\left(\frac{P}{P_0}\right) \tag{1.1}$$

where N is the sound pressure level in decibels (dB), P is the receiver sound pressure and P_0 is a reference sound pressure, usually taken as the international standardized human minimum audible threshold of $20\ \mu$Pa.

On the contrary, noise reflects the human, commonly unwanted, reaction to sound and there are certain side-effects associated with it. Those effects will be described in the following sections, as well as, the different measures implemented with the aim of quantifying noise more accurately.

1.1.1. Effects of noise

Accordingly to [7], there are many different effects of noise on people and individuals experience them to differences degrees. As shown in Figure 1.1, the effects fall into two main categories; behavioural and physiological effects. On the one hand, physiological stand for health effects which include noise-induced hearing loss and other indirect risks to the physiological and psychological well being. As mentioned in the aforecited document, hearing loss is well documented and is not considered likely to be caused by the levels of aircraft noise experienced beyond airport boundaries. In addition, although it is true that noise can cause different biological reflects and responses, there is no proof that this could lead, over time, to clinical recognizable illness.

Behavioral reactions, in turn, are characterized by being more subjective and very sensitive to non-acoustic socio-psychological factors such as location or state of well-being. As a strong influence of acoustical and non-acoustical factors exists, it is quite difficult to define the underlying noise-response relationships.

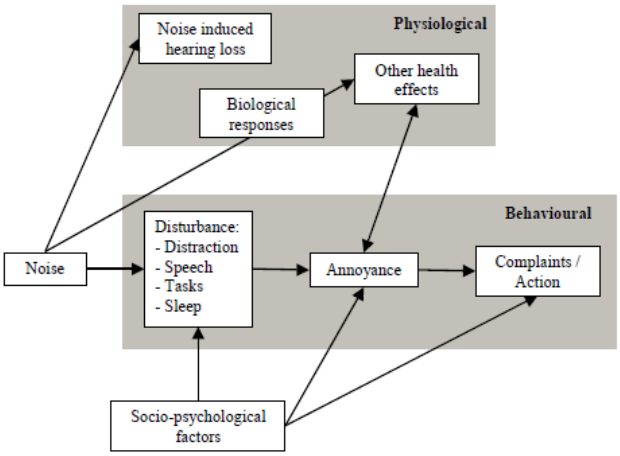

Figure 1.1: General cause and effect relationships [7]

That is why a lot of research is being focused on understanding the long-term, and also short-term, relationships between noise and human responses. For example, [8], implements a model for synthesizing aircraft flyover noise in order to provide a better solution for comparing noise abatement procedures and consequently improve the communication between the operators, airports, and communities. For further information on Noise effects, see [7, chapter 3.1].

1.1.2. The A-weighted sound level

As a consequence of the intrinsic characteristics of noise, human perception of loudness is highly nonlinear, therefore the relationship between frequency, intensity, and loudness is quite complex. The International Organisation for Standardisation (ISO) has a unit called the Phon, which describes (subjective) loudness. Figure 1.2(b), shows a plot o equal-loudness contours as a function of the frequency in Hz and the Sound pressure level in dB.

As it can be seen, the human perception of noise is significantly sensitive to the frequency spectrum, which implies the need of a corrector factor to correlate overall sound pressure with the frequency sensitivity of the human ear. The European Civil Aviation Conference (ECAC) describes two main scales for correcting (or weighting) aircraft noise sound pressure level; the A-weighted sound level (L_a) and the Tone-corrected Perceived Noise level (L_{pnt}).

The A-weighting is described as a simple filter applied to sound measurements which applies more or less emphasis to different frequencies in order to mirror the frequency sensitivity of the human ear at a moderate sound energy level (see Figure 1.2(a)). It is universally used in environmental noise level studies, and especially on most of the aircraft noise monitoring applications. The resulting unit of the A-weighting is the dB(A).

On the other hand, tone-corrected perceived noise levels bring in a broadband of sources containing pure tones and other spectral irregularities. It is used uniquely for precision aircraft noise measurement, which is confined to aircraft design and certification.

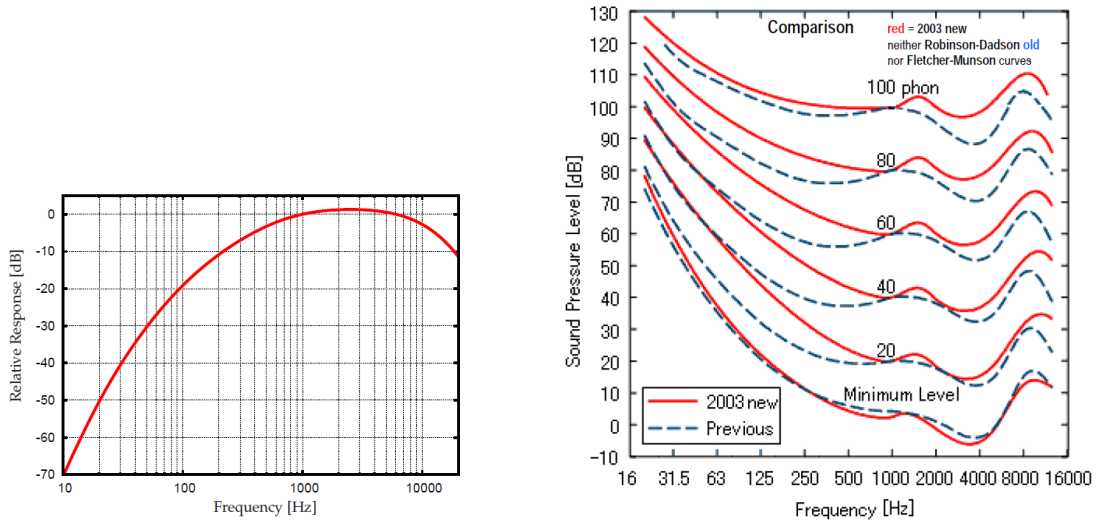

(a) A-weighting scale [5]

(b) Equal-loudness contours [9]

Figure 1.2: Different NAPs optimizations

1.1.3. Aircraft Noise

There are two main categories concerning aircraft noise; airframe and engine noise. Airframe noise is considered as the sound generated by all the non-propulsive components of an aircraft. Accordingly to [10, 5] there are five main mechanisms contributing to airframe noise:

- the wing trailing-edge scattering of boundary-layer turbulent kinetic energy into acoustic energy;
- the vortex shedding from slat/main-body trailing-edges and the possible gap tone excitation through nonlinear coupling in the slat/flap coves;
- the flow unsteadiness in the recirculation bubble behind the slat leading-edge;
- the roll-up vortex at the flap side edge; and
- The landing-gear multi-scale vortex dynamics and the consequent multi-frequency unsteady force applied to the gear components.

As opposed to airframe noise, jet engine noise is related, as its name implies, only to the noise produced by the aircraft engines, which could be subdivided into the sound emitted by the four main components of the engines: compressors, turbines, combustion chamber and exhaust nozzle.

Thus, during the departure phase, when thrust is at his maximum setting, noise engine is the predominant source of noise. Nevertheless, during the approach phase, the main source of noise comes from the airframe, as thrust levels are very low and engine noise does not mask the airframe contribution anymore. This being said, modeling aircraft noise for departure or landing route has two completely different approaches. On one hand, for departure scenarios, the noise model needs to his attention on power plant noise emissions, whereas for landing scenarios, the noise model needs to incorporate different aerodynamic configurations, such as different flap and slats configurations.

1.2. Noise Reduction Measures

Reference [11] identifies three different levels when addressing the air traffic noise exposure problem. The first or “primary level”, brings in improvements in engine and aerodynamic construction technology in order to reduce the noise emitted from the source. The second, or “secondary level”, incorporates changes in arrival and departure procedures in order to achieve a significant reduction in the noise impact by means of more environmentally-friendly trajectories. Last but not least, at the “tertiary level”, “the noise exposure problem is related to restrictions introduced by individual airports and/or aviation authorities”. Figure 1.3 shows different existing measures and the number of airports which incorporated them in 2009.

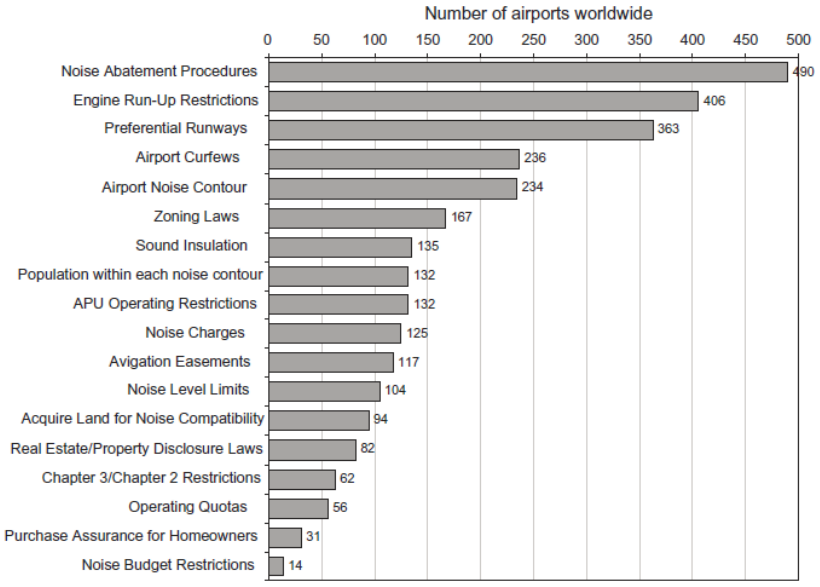

Figure 1.3: Number of airports worldwide having introduced some of the noise reduction measures, in the year 2009 [11]

In this project, the “secondary level”, where noise impact is reduced by means of changing arrival and departure procedures, will be tackled. Those procedures receive the name of Noise abatement Procedures or NAPs. In his study, [5] splits them into two big categories. On one hand, those strategies that are designed manually by one or several experts according to empiric data collected in the past and previous experience obtained by themselves. On the other hand, there are those strategies that compute, using different mathematical methods, automatically or semi-automatically optimal noise abatement procedures drawn from a set of imposed constraints and objectives.

1.2.1. Noise abatement Procedures (NAPs)

Accordingly with [11], noise abatement procedures are fundamentally based on two requirements:

- Maximizing the distance between affected zones and the aircraft for as long as possible (higher climb and descent rates)

- Minimizing the generated noise at source (flying with lower engine power)

Lots of different NAPs are currently being implemented in airports around the globe and can be segregated in three main categories; those concerning the management of vertical trajectories, those where the lateral trajectory management is assessed and those where a combination of both is implemented with the aim of obtaining a better performance [5].

With the inclusion of Area Navigation (RNAV) a new window of opportunities was opened regarding the conventional approach of navigation based on over-flying radio navigation aids. Also, features like the Radius to fix (RF) Path terminator increased the accuracy offered by the RNAV system, decreasing the dispersion around the nominal track (See Figures 1.4(a) and 1.4(b)). As another example, Figure 1.4(c) shows the current implementation of an RF procedure at the Ronald Regan National Airport. As the image shows, the procedure overflies the Potomac River in order to mitigate the noise impact over the population.

In cases where lateral adjustment is not possible, acting in the vertical plane is an efficient alternative to mitigate aircraft noise. For the departure phase, the International Civil Aviation Organization (ICAO) Noise Abatement Departure Procedures (NADP) [12] is one of the most established methods. The procedure specifies the airspeed profile that should be maintained during climb as well as the altitude points where thrust/power reduction may be done. However, these procedures are generic and not always fit into the specific scenarios that a certain airport may suffer.

Regarding the approach phase, several techniques are currently being implemented. It is worth mentioning that nowadays the final approach segment is straight and aligned with the extended runway centerline, which constrains the range of feasible solutions in the lateral domain. Nevertheless, there is space for optimizing the route during the arrival and the initial approach phases.

Some strategies propose changes in the final constants slope straight segment mentioned before. Increasing the Instrument Landing System (ILS) interception altitude or imposing a higher glide-slope angle are two of the most common implementations. Other solutions try to reduce the airframe noise by driving the aircraft in clean configuration (i.e. with flaps and slats retracted) and with the landing gear[1] retracted for as long as possible. Those procedures are called Low Drag Low Power (LDLP) approaches.

Another state-of-the-art-solution implements the use of Continuous Descent Approaches (CDA), where the aircraft performs an interrupted thrust-idle flight until a point before the ILS-Localiser interception. The optimal vertical profile defining the CDA depends, apart from the aircraft type, on several variables, such as the aircraft weight, the present wind conditions, the cost index, etc.

Once the descent has started, as each aircraft has a unique optimal descent profile, there exists a lot of uncertainty regarding the aircraft position, height and velocity. For this reason, as giving instructions while performing the descent is not feasible, as it will stop the CDA, air traffic controllers impose larger separation distances between airplanes with the aim of maintaining security standards, thus, as a result, airport capacity is significantly reduced.

[1] The landing gear not only adds noise by its airframe noise character but by means of increasing the engine noise as more thrust is needed to compensate the generated drag [5].

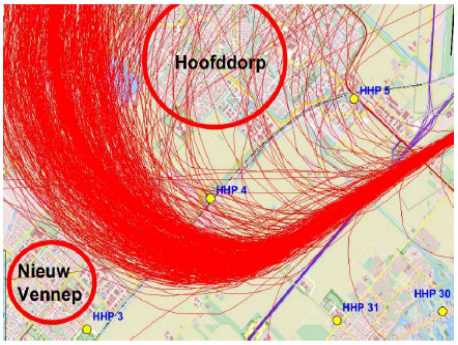

(a) Flight tracks using conventional and RNAV navigation with no RF leg capability

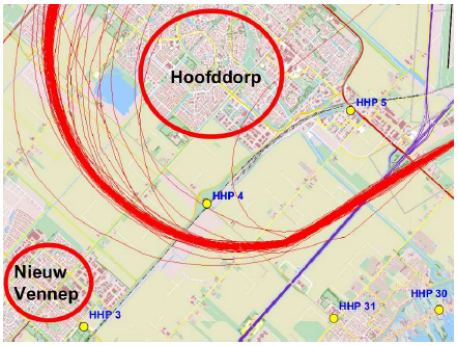

(b) Flight tracks with RF leg capability

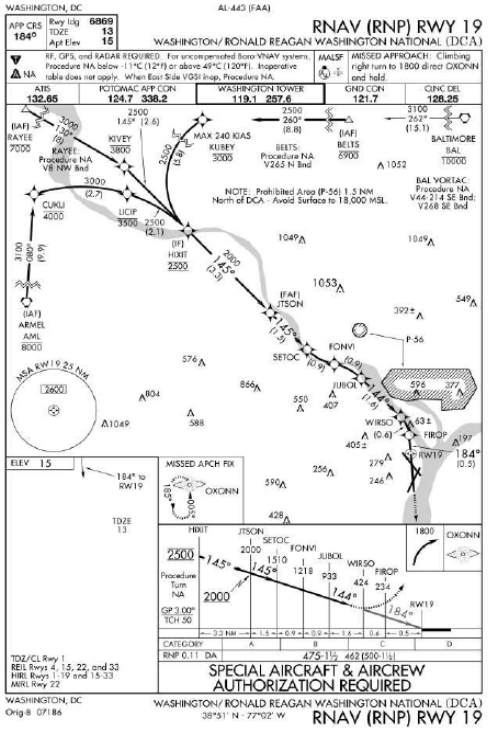

(c) Example of an RNAV approach with RF legs at Ronald Regan National Aiport

Figure 1.4: Examples of Noise Abatement Procedures [5]

With the objective of maintaining airport capacity when implementing CDAs, a lot of active research is currently going on in aircraft trajectories prediction [13, 14, 15, 16, 17].

1.2.2. NAPs optimization

Even though the aforementioned NAPs have proven their effectiveness in reducing the impact of aircraft noise, those procedures are implemented individually as there is no certain knowledge of how they should be combined. Consequently, raises the need for an optimal noise abatement procedure that takes into account all the variables playing a role in the trajectory definition. Due to the fact that the optimization of NAPs is a relatively new field, a big variety of proposals and strategies can be found. On the following section, a brief review of the currently available literature will be exposed, addressing four main characteristics of NAPs optimizers; noise models, measurement grids and cost functions strategies and different numerical approaches.

1.2.2.1. Noise models

When implementing a noise model, a trade-off between the computational cost and the accuracy of the model must be taken into account. As [18] states; “The high mathematical complexity associated with the computation of emission and propagation of aircraft noise limits the adoption of accurate models to offline optimization studies, typically performed

to optimize the departure and approach paths to aircraft, which are the portions of the flight in close proximity to the ground". In addition, explains that, due to some opportune assumptions, the integration of simplified models such as the Noise-Power-Distance (NPD) models with a simplified worst-case emission and with a Demographic Distribution (D3) and Digital Terrain Elevation (DTED) databases can enable a quasi-real-time noise model implementation. The most widely used NPD model is the Integrated Noise Model (INM) from the Federal Aviation Agency (FAA), which can be found in several studies such as [19, 5, 18].

The INM is based on the European Civil Aviation Conference (ECAC) document 29 3rd Edition from the ICAO and uses a grid-based approach for computing noise footprints. An NPD table is given from which noise is computed for a given distance and power setting. The values are calculated based on interpolation from the NPD table, which contains empirical measurements for each aircraft type under reference conditions.

A very similar new implementation of the ECAC rules is given by the Eurocontrol Aircraft Noise and Performance (ANP) databases. The ANP is the free of cost alternative to the INM even though is also based on the same above-mentioned ICAO document. Although it has the same structure as the INM, the ANP database is not as complete as the INM database and has fewer settings options. As an example, the INM database offers 4 flight aerodynamic configurations, whereas the ANP database only offers Arrival and Departure configurations.

For more details on the ANP and INM databases refer to [7, 20].

1.2.2.2. Measurement grids and cost functions

Once the noise model is implemented, a cost function must be defined in order to optimize the aircraft trajectory. When dealing with NAPs optimization, one of the crucial aspects to take into account is the allocation of the observer(s), also known as measurement grid. As noise models like the INM are specially conceived for computing noise prints by means of a grid-based approach. The first intents implemented a grid of points, or "microphones", where noise was measured [2, 3]. Although this is one of the most accurate ways of estimating the noise print over an area, the computational cost of this kind of implementation is quite considerable.

Trying to minimize it, [21, 22] implemented a set of sensitive areas which borders were defined by a set of points (Figure 1.5(b)). By doing this, while ensuring that the noise constraints were fulfilled inside the sensitive areas, the number of points was considerably reduced as well as the computational cost. Other studies opt for a less accurate but yet more simple solution, such as placing one microphone for each town located near the airport [23] or just imposing a Noise Sensitive Area (NSA) which should not be overflown (Figure 1.5(a)).

In cases where more than one point of measurement is used, a proper way of combining them must be achieved. As more than one objective has to be taken into account, the optimization problem falls into the multi-objective optimization problem class. First efforts, just evaluated the noise print as a whole, adding all the measures, and displaying the mean as the cost function [2]. Others applied different weightings to each of the measurements, basing the weighting in the density of the population or the number of awakenings [3, 4]. Some studies added more complex algorithms in order to add equity to the cost function.

For instance, Ref. [21], applies what he calls the min-max approach: whereas most of the multi-objective cost functions present in the literature tried to minimize the whole impact of the trajectory, Prats centered his approach in reducing the noise impact there where it was worst, as he stated that this was the fairest way of addressing noise abatement procedures.

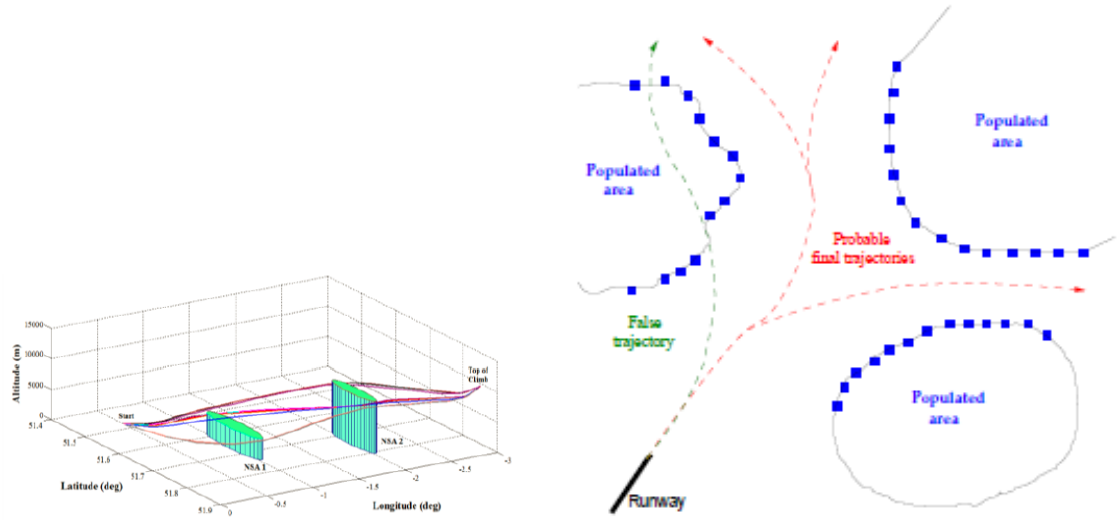

(a) NSA-based optimization [18]

(b) Noise sensitive areas definition [5]

Figure 1.5: Different NAPs optimizations

1.2.2.3. Numerical Methods

According to [5], "the optimization of an aircraft trajectory, as a 4-dimensional continuum, is a constrained optimal control problem". These kind of problems are not easy to solve, due to nonlinear functions appearing in the definition of the optimization objective and constraints. For this reason, there exist several techniques currently being implemented aiming to solve this optimization problem in the most efficient way possible.

First intents tried to solve this type of problems analytically, offering feasible solutions for small and simplified optimization problems [24]. Unfortunately, NAPs optimization does not fall into this category. That is why, as computers started to be more powerful, also numerical methods started to become the preferred solution in order to solve this kind of problems. A lot of different numerical methods can be found aiming to solve the problem stated before; Stochastic methods and gradient-based approaches, are within the most commonly found methods.

Stochastic methods incorporate random elements in the algorithm with the purpose of finding an optimal solution. Those kinds of methods can be divided into several different types, such as genetic and ant colony algorithms, which are inspired by biological and natural processes. Nevertheless, when an optimal solution is found those methods are not good proving that the corresponding solution is the global optimal and the computational burden is also considerable.

Therefore, gradient-based approaches will be chosen for this project. There are two main categories concerning gradient-based algorithms; direct shooting and direct collocation

methods, where direct collocation methods have been elected as the approach implemented in this project.

Direct collocation methods consist on a discretization of the whole equations set defining the problem in order to transform the initial continuous optimal control problem into a set of discretized states and controls which with the different constraints imposed, define the set of variables and constraints of a new Non-Linear Programming (NLP) problem. Then, the remaining NLP problem can be solved using non-linear programming algorithms such as the ones implemented in the CONOPT solver, which will be introduced later.

However, it is worth mentioning that the main drawback of direct methods is the lack of certainty when the problem to solve is non-convex since one cannot guarantee that a globally optimal solution is attained. Furthermore, the solution obtained will be very sensitive to the input parameters (guesses) given at the beginning of the optimization [5].

CHAPTER 2. MODEL

When performing the optimization of a noise abatement trajectory, it is important to define accurately the model describing the aircraft noise emission and its propagation, as well as, the aircraft dynamics. That being said, in this chapter, the adopted method for computing aircraft noise will be explained, in addition to a new technique for measuring the noise impact of an aircraft trajectory. Finally, the model describing the aircraft dynamics and performance will be introduced.

2.1. Noise Model

In order to proceed with the optimization, an aircraft noise model is needed to compute the perceived noise levels for a given flight trajectory. As explained in section 1.2.2.1., the Integrated Noise Model (INM) from the Federal Aviation Administration (FAA) is generally adopted in several scientific studies [5, 18, 25].

Although INM is widely used, the Aircraft Noise and Performance (ANP) database, a similar, free of charge, alternative, has been finally implemented. As explained, in section 1.2.2.1., the ANP model offers the same simplicity of implementation found in the INM, which has been the main point borne in mind when choosing a noise model for the optimization process.

This being said, in the next section, the exact computation of the noise values based on the ANP NPD tables will be discussed.

2.1.1. Single event noise level general expression

Although several metrics for quantifying noise exposure exists, for this project the maximum A-weighted sound level (LAMAX or L_{max}) will be considered. The L_{max} metric takes as noise value the maximum level of a single fly-over measured in dB(A), which is the most convenient metric for modeling the human sensitivity to different frequencies (see section 1.1.2.). The difference between noise metrics will not be discussed in this document, for more information on noise metrics see [7, chapter 3.2].

Thus, the maximum sound level at a given location i will be expressed as $L_{max,i}$ and it is defined by:

$$L_{max,i} = \max_{t}[N_i(t)] \tag{2.1}$$

where $N_i(t)$ is the sound pressure level at a location i as a function of the fly-over time t.

As the NPD data provided in the ANP database is normalized to reference day atmospheric conditions, an acoustic impedance adjustment is given in order to adapt the data to specific weather conditions. “Acoustic impedance is related to the propagation of sound waves in an acoustic medium and is defined as the product of the density of air and the speed of sound” [20]. However, as it is explained in the document, the effect of the acoustic impedance on the noise computation is easily negligible. “In particular, it should be noted that under the standard atmospheric conditions (p_0 = 101.325 kPa and T_0 = 15.0 °C), the

impedance adjustment is less than 0.1 dB (0.074 dB). Since the purpose of this project is to obtain a first preliminary result, the impedance adjustment will be neglected, although it could be included in future work, if desired.

Thus, the maximum noise level, between an aircraft on a fixed point of its trajectory and the receiver at a given location i, can be approximated using the ANP model as:

$$L_{max,i} \simeq L_{max,i}^{NPD} + N_i^l \tag{2.2}$$

where $L_{max,i}^{NPD}$ is the obtained L_{max} value from the NPD table, and N_i^l is the correction value which takes into account the lateral attenuation and engine installation correction terms. Both are computed as a function of the slant distance, the euclidean distance between the aircraft and the point i, and will be further explained in section 2.1.2. and 2.1.3..

2.1.2. Correction terms

There are two main correction terms that must be taken into account accordingly with the ECAC recommendations. The first one is the lateral attenuation adjustment, which takes into account the scenario where the aircraft trajectory is not over-flying vertically at a given point i. The second one is the engine installation correction factor, which takes into account the angle where the aircraft engines are pointing regarding the position of the receiver. Both terms are subtracted as follows:

$$N_i^l = \Delta_I(\varphi) - \Lambda(\beta, l) \tag{2.3}$$

where Δ_I and Λ are the engine installation and lateral attenuation correction factors, respectively.

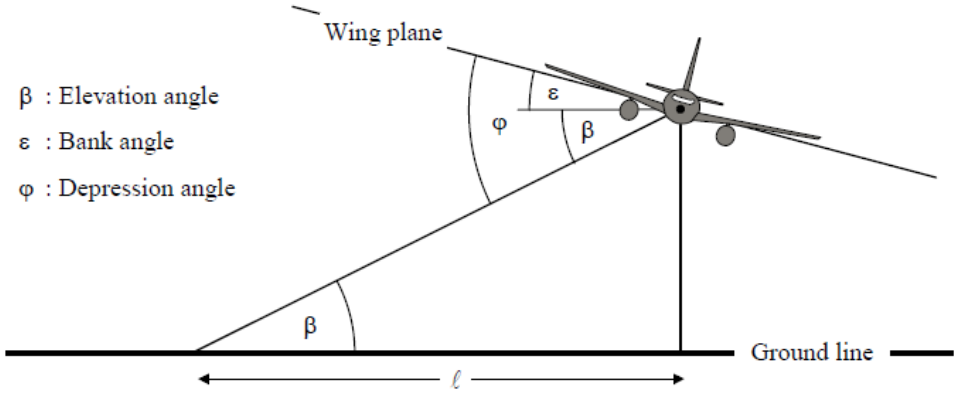

Figure 2.1: Aircraft-observer angles in plane normal to flight path [20]

When flying, the noise radiation patterns of an aircraft are influenced by the location of the engines. Processes like refraction, reflection and scattering are found when the engine noise encounters the solid surfaces and the aerodynamic flow fields of the aircraft. As a result, a non-uniform directionality of sound radiated laterally about the roll axis of the aircraft is obtained, and can be described as:

$$\Delta_I(\varphi) = 10\log\left(\frac{\left(a\cos^2\varphi + \sin^2\varphi\right)^b}{c\sin^2\varphi + \cos^2 2\varphi}\right) \tag{2.4}$$

where ϕ is the depression angle described in Figure 2.1, and a, b and c are known coefficient values given by the ECAC document (Table 2.1). There exist two main configurations for which different coefficients are provided; wing-mounted engines and fuselage-mounted engines.

Table 2.1: Engine installation correction parameters [20]

	a	b	c
Wing-mounted engines	0.00384	0.0621	0.8786
Fuselage-mounted engines	0.1225	0.3290	1

Figure 2.2 shows the radiation pattern for both configurations. As it can be seen, for fuselage-mounted jets the difference between the uncorrected pattern and the corrected one are priceless (less than 2 dB in the worst scenario). Thus, in order to simplify things when computing the first tests our noise model will neglect the engine installation factor. However, the architecture of the exposed model enables the implementation of this factor if desired.

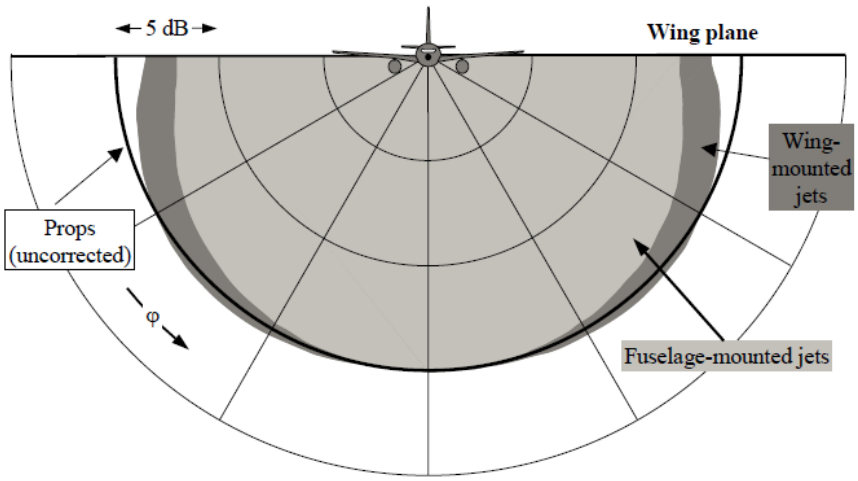

Figure 2.2: Lateral directivity of installation effects [20]

As its name implies, Λ takes into account the lateral attenuation adjustment for cases where the aircraft trajectory is not over-flying vertically the location i, and is modeled as follows:

$$\Lambda(\beta, l) = \Gamma(l) \cdot \zeta(\beta) \tag{2.5}$$

with $\Gamma(l)$ being a factor dependent on the lateral distance between the aircraft and the receiver (l), and given by

$$\Gamma(l) = \begin{cases} 1.089[1 - \exp(-0.00274l)] & \text{for } 0 \leq l \leq 914 \text{ m} \\ 1 & \text{for } l > 914 \text{ m} \end{cases} \tag{2.6}$$

and $\zeta(\beta)$ being the long-air-to-ground attenuation given by

$$\zeta(\beta) = \begin{cases} 1.137 - 0.0229\beta + 9.72\exp(-0.142\beta) & \text{for } 0^\circ \leq \beta \leq 50^\circ \\ 0 & \text{for } 50^\circ \leq \beta \leq 90^\circ \end{cases} \tag{2.7}$$

where β is the elevation angle shown in Figure 2.1

It is worth mentioning that ANP and INM databases are specially conceived for computing airport high accuracy noise prints. For this reason, noise is modeled during phases where the aircraft is considerably low. As the proposed optimization process developed in this project stops once the ILS is intercepted, those factors that model low height acoustics can be neglected without compromising seriously the accuracy of the results.

Figure 2.3 shows the graphical representation of the lateral attenuation l. Within the noise modeling community, exists quite a consensus in neglecting the lateral attenuation factor for elevation angles greater than 12° [25]. Thus, for this project, the worst-case scenario will be taken into account and the lateral attenuation coefficient will also be neglected, which simplifies, even more, the model.

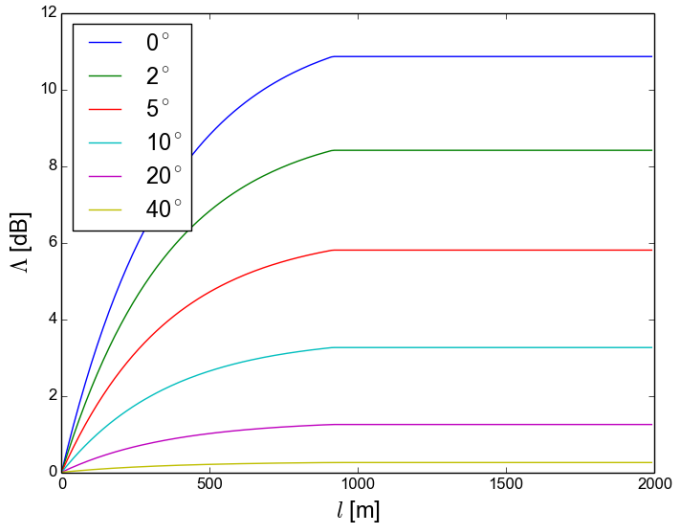

Figure 2.3: Lateral Attenuation factor plot

2.1.3. The Noise Power Distance Curve

The ANP database offers different Noise Power Distance (NPD) tables given three different parameters, which are: the aircraft type, the flight configuration (Departure or Landing) and the desired noise metric. Each NPD table gives the noise value for a given slant distance (distance from the aircraft to the observer) d, and a given power setting P, which units may change for the different tables. Figures 2.4(a) and 2.4(b) show the Lmax curve obtained for the Boeing 747-400 aircraft in landing and departure configurations.

Notice how the number of points and the ranges of the input variables vary for the two configurations, giving different resolutions for each table. For this reason, the ECAC 29 3rd document provides a set of rules for the interpolation and extrapolation of the provided NPD curve. As an example, Equation 2.8 shows the expression provided by the document for the slant distance values that lie outside the boundaries of the NPD table. By employing a logarithmic extrapolation, the expression estimates the noise level for a given slant distance d, where $L^{NPD}_{max,i}(d_I)$ and $L^{NPD}_{max,i}(d_{I-1})$ are the last two noise levels tabulated.

$$L^{NPD}_{max,i}(d) = L^{NPD}_{max,i}(d_{I-1}) - \frac{L^{NPD}_{max,i}(d_{I-1}) - L^{NPD}_{max,i}(d_I)}{\log(d_I) - \log(d_{I-1})} \cdot (\log(d) - \log(d_{I-1})) \tag{2.8}$$

On the other hand, the interpolation and extrapolation, for different power settings, follow a linear expression. Equation 2.9 shows the formula needed to compute Noise levels that lie within the NPD curve; where P_I and P_{I+1} are the closest two tabulated values.

$$L^{NPD}_{max,i}(P) = L^{NPD}_{max,i}(P_I) + \frac{L^{NPD}_{max,i}(P_{I+1}) - L^{NPD}_{max,i}(P_I)}{P_{I+1} - P_I}) \cdot (P - P_I) \tag{2.9}$$

Thus, accordingly with the ECAC document an interpolation and extrapolation of the ANP NPD curves have been conducted in order to extend the given curves to the desired boundaries, covering up all the possible scenarios during the trajectory and smoothing the transition between points. Figure 2.5(a) shows the resulting NPD curve, in arrival configuration, after the extrapolation and interpolation process, which ensures that the Noise level could be obtained during the whole trajectory.

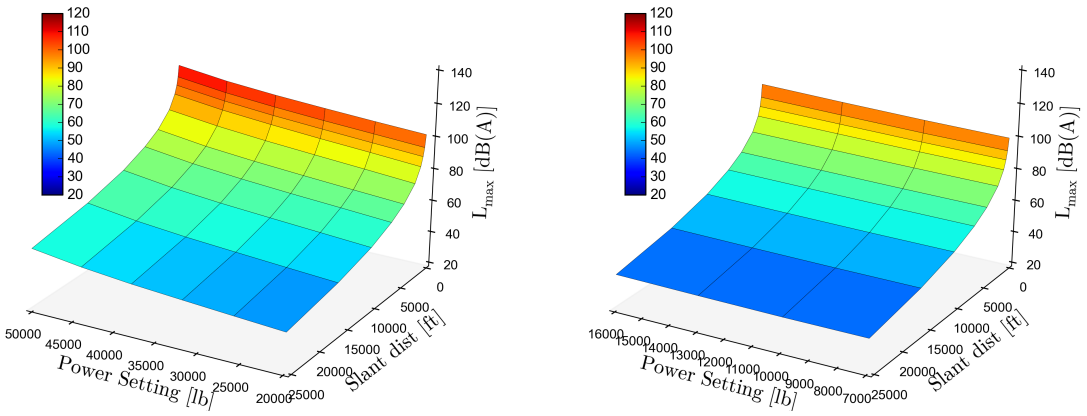

(a) Departure Configuration

(b) Arrival Configuration

Figure 2.4: B747-400 L^{NPD}_{max} curves

A final correction to the NPD curve must be done before we proceed with the noise computation. There is no need for the optimizer to take into account noise annoyance under a certain noise threshold where the ambient noise could be higher. That's why the NPD curve values are limited, in this case, to 40 dB(A). This means that all the values under the 40 dB(A) threshold will be imposed to be equal to 40 dB(A). By doing this, all the values under the threshold will be treated equally, from the optimizer point of view, and as a result, the cost function will minimize the route just taking into account those points of the trajectory where the noise emitted on the NSAs is higher than the threshold.

The 40 dB(A) threshold is imposed as a first guess, as it is considered to be a more than strict value. However, this threshold is considered to be an important parameter in the optimization process and some results with different values will be exposed on the results. This said, Figure 2.5(b) shows the final extrapolated NPD curve with the 40 dB(A) threshold value imposed.

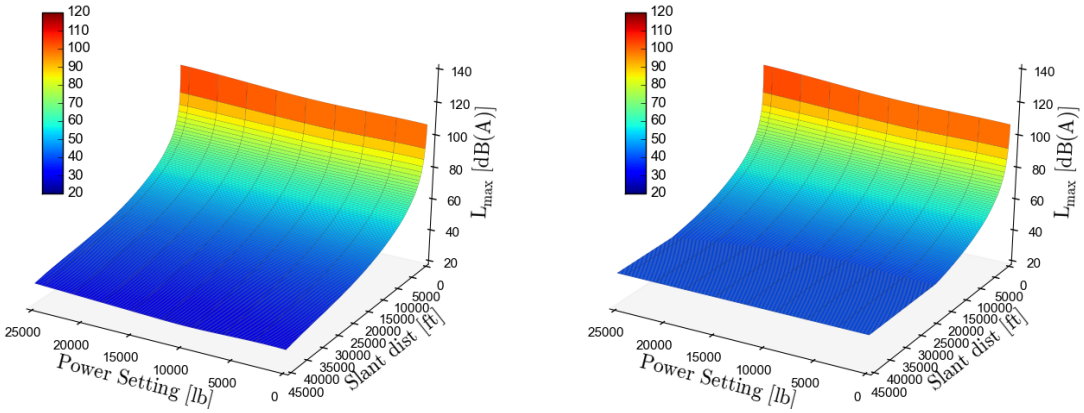

(a) no threshold (b) 40 dB(A) threshold imposed

Figure 2.5: B747-400 L_{max}^{NPD} curves extended

As a result, a final surface $L_{max}(P,d)$ from which the Noise level $L_{max,i}$ can be obtained as a function of the slant distance d and the power setting P. This surface will be introduced to the optimizer as a mathematical function generated as a continuous and differentiable function expressed in the form of a spline, which implementation will explain in the next chapter.

2.2. Measurement grid

As mentioned in section 1.2.2.2., one of the most important aspects to take into account when dealing with the optimization of noise abatement procedures is the measurement grid, the space where noise levels will be measured in order to optimize the aircraft trajectory.

In chapter 1.2.1. it was shown how, in concordance with [11], noise abatement procedures are based on two requirements, one of them being to maximize the distance between the aircraft and the affected zones. Based on this principle and on [5], the proposed method is going to incorporate a series of noise sensitive areas (NSAs) where the noise print should be minimized. Following the methodology implemented in [5], noise will be computed exclusively at the border of the noise sensitive area, assuming that if the noise level constraint is fulfilled at the border it will be lower inside the area.

However, as it was shown in figure 1.5(b), defining those NSAs borders with points is often complicated as a large number of points drawing the border increases the computational cost considerably, but if it is too small, the optimizer could take an infeasible trajectory entering an NSA. For this reason, although using a grid of points is the most established method, in this project a novel technique will be presented which replaces the discretized

points by a continuous function describing, for each north-east coordinate, the distance l to the closest NSA. Simplifying, then, the optimization process by means of giving only one noise level for each point of the trajectory, in comparison to other methodologies where multiple measurements are taken into account.

2.2.1. Contour computation

As shown in 2.1.3., the perceived noise at a given i location is computed primarily taking into account the slant distance and the power setting. Whereas the power setting is completely independent of the measurement grid, the slant distance as its own definition implies is not. The slant distance is defined as the Euclidean vector joining the position of the aircraft and the observer, and can be divided into two main components; the lateral distance (l) and the height (h) separating them, see Figure 2.1.

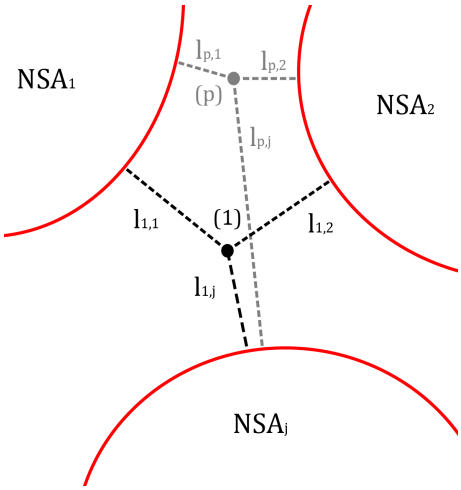

Figure 2.6: Lateral distance surface computation scheme

Before proceeding, it is worth mentioning that a strong assumption is made when computing the height distance. All measurement points are assumed to be located at sea level. Although this is the first intent of solving the problem, is a strong assumption which could lead to significant differences between the predicted noise level and the real value and an important point to bear in mind on future work.

That said, being defined a set of noise sensitive areas as $\{NSA_1, NSA_2, ..., NSA_s\}$ a lateral distance $l_{p,j}$ will be computed from a point p defined by a couple of north-east coordinates, to the closest point of the border of each NSA_j area (see figure 2.6). Equation 2.10 shows the resulting matrix L_{NSA}, containing all the different $l_{p,j}$ values computed for every point p in the grid to every NSA_j.

$$L_{NSA} = [l_{p,j}] = \begin{bmatrix} l_{1,1} & l_{1,2} & \cdots & l_{1,s} \\ l_{2,1} & l_{2,2} & \cdots & l_{2,s} \\ \cdot & \cdot & \cdots & \cdot \\ l_{M,1} & l_{M,2} & \cdots & l_{M,s} \end{bmatrix} \tag{2.10}$$

Thus, as the principal objective is to compute the noise value at the most sensitive location, for every point of the trajectory, only the shortest distance from all the set is retained:

$$l_{NSA}^{(p)} = \min_{j} (L_{NSA}) \tag{2.11}$$

Where $l_{NSA}^{(p)}$ is the resulting vector of length M, containing the lateral distance to the closest NSA for each point p.

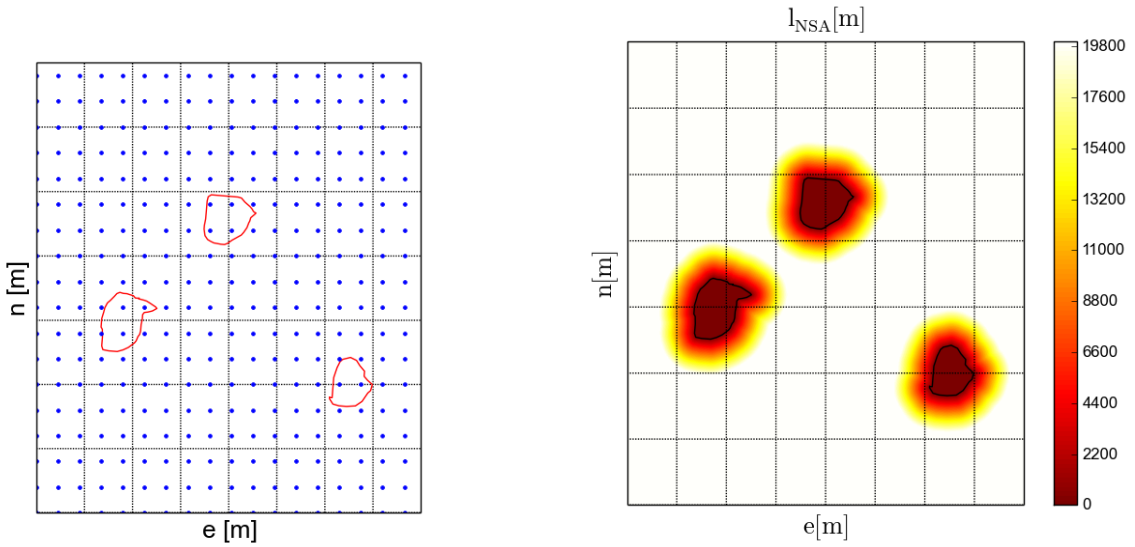

(a) Example grid and NSAs (20x20 points)

(b) Final obtained surface (260x260 points)

Figure 2.7: Lateral distance surface example

Figure 2.7(a) shows an example of a 20x20 grid of points p for which the lateral distance l_{NSA} will be computed accordingly to the three red NSAs defined. On the other hand, figure 2.7(b) shows the final result obtained, this time for a 260x260 grid which ensures a better definition of the contour. As it can be seen, the lateral distance l_{NSA} is given in meters and there is a threshold value of 20 km, due to the fact that noise levels for distances higher than 20 km are negligible for all the possible scenarios.

As the reader may have noticed, the presented contour is not a continuous function as it is formed by discrete points each one containing a l_{NSA} value. In order to use the contour in the optimization of the trajectory, the surface has to be smooth and continuous. For this reason, as well as it was done in section 2.1.3., the contour defined by the two coordinates north-east of each point p, and its respective l_{NSA} value, will be approximated as a mathematical function defined by spline fitting methods.

As a result, a function $l_{NSA}(n,e)$ is obtained, where the lateral distance to the closest sensitive location is known at every north-east coordinates. Details on how this surface is implemented in the optimization process will be given in the next chapter.

2.2.2. Aircraft trajectory noise level

Computing a unique noise level value for each point in the trajectory differs quite a lot from past work done in this field, where noise was measured at the same time in different

points (see section 1.2.2.). Thus, in order to make clear the methodology applied, the exact computation of noise for each point of the trajectory needs to be explained.

The noise level at the closest NSA will be estimated in concordance with equation 2.2, where the L_{max} noise level was computed for a given location i. As mentioned, in section 2.1.2., all the correction terms will be neglected for different reasons. Thus, the L_{max} for each location i will only depend on the L_{max}^{NPD} value which as explained in section 2.1.3. depends on the power setting P and the slant distance d:

$$L_{max,i} = L_{max,i}^{NPD}(P, d_i) \tag{2.12}$$

where the slant distance can be computed by means of the Pythagorean formula, taking as cartesian coordinates, the lateral distance l and the height h between the aircraft and the receiver. As mentioned before, all the NSAs will be considered to be at sea level, thus, only the aircraft pressure altitude h_p taking into account International Standard Atmosphere (ISA) conditions, will be considered. This said, the slant distance can be computed as follows:

$$d_i = \sqrt{l^2 + h^2} = \sqrt{l^2 + (h_p - h_i)^2} \approx \sqrt{l^2 + h_p^2} \tag{2.13}$$

where h_i is the elevation of the measurement location, which will be neglected.

This could be the methodology applied if noise would be computed at different discrete locations i. However, as explained in the last section, a continous function $l_{NSA}(n, e)$ where the lateral distance to the closest NSA has been computed. Then, both, equation 2.12 and 2.13 can be redefined by means of the aircraft trajectory north-east coordinates which will change with time.

$$L_{max}(t) = L_{max}^{NPD}(P(t), d(t)) \tag{2.14}$$

$$d(t) \approx \sqrt{(l_{NSA}(n(t), e(t)))^2 + (h_p(t))^2} \tag{2.15}$$

As a result, the L_{max} value to the closes NSA is computed continuously through time, and is not restricted to specific north-east coordinates, which simplifies the implementation of the measurement space at the same time, it offers the estimation of the noise impact produced by the aircraft trajectory.

2.3. Aircraft Dynamics

Trajectory optimization requires a well-defined mathematical model describing the aircraft dynamics and performance with enough fidelity to conduct studies on current Air Traffic Management (ATM) scenarios.

There are several models which describe the motion of a flying aircraft, as in noise modeling; there exists a compromise between the accuracy of the model and its complexity. For this reason, point-mass models, where the aircraft is described as a point-mass object and all the rotational forces are neglected, are chosen over more complex models such

as the rigid-body model where those forces are taken into account adding a large number of dimensions and short period modes, which as a result increase significantly the model complexity and the execution time of the optimization algorithms [19].

In addition to neglect rotational forces considering only the translational motion of the aircraft, two more simplifications are taken into account: turn maneuvers are considered to be executed in a coordinated way (imposing a null sideslip angle) and a flat non-rotating earth is also assumed.

This being said, the aircraft trajectory dynamics and kinematics can be described by a set of non-linear equations, defined by the following state-space representation:

$$\begin{cases} \frac{\mathrm{d}v}{\mathrm{d}t} = \dot{v} = \frac{1}{m}\left[T(t) - D(t) - mg\sin\gamma(t)\right] \\ \frac{\mathrm{d}\chi}{\mathrm{d}t} = \dot{\chi} = \frac{g}{v(t)}\left[\frac{n_z(t)\sin\mu(t)}{\cos\gamma(t)}\right] \\ \frac{\mathrm{d}\gamma}{\mathrm{d}t} = \dot{\gamma} = \frac{g}{v(t)}\left[n_z(t)\cos\mu(t) - \cos\gamma(t)\right] \\ \frac{\mathrm{d}e}{\mathrm{d}t} = \dot{e} = v(t)\sin\chi(t)\cos\gamma(t) + W_e \\ \frac{\mathrm{d}n}{\mathrm{d}t} = \dot{n} = v(t)\cos\chi(t)\cos\gamma(t) + W_n \\ \frac{\mathrm{d}h_p}{\mathrm{d}t} = \dot{h_p} = v(t)\sin\gamma(t) + W_h \end{cases} \tag{2.16}$$

where T is the aircraft idle thrust; g is the gravity acceleration constant; γ, μ and χ are the aerodynamic flight path, bank and heading angles, respectively; v is the true airspeed (TAS); m is the aircraft mass; h_p is the aircraft pressure altitude; n and e are respectively the northward and eastward coordinates; n_z is the vertical load factor (defined as $n_z = \frac{L}{mg}$) and D is the aerodynamic drag.

The wind field will be neglected for the scenarios that will be conducted on this project, thus the three wind components in equation 2.16; W_e, W_n and W_h, will be set to zero. Nevertheless, the possibility of adding a known and steady field is implemented on the aircraft dynamics and could be used in future studies. Notice that the aforementioned wind field is only implemented in the aircraft dynamics, not in the noise model. Thus, it will not have any effect on the sound propagation. For more information of the effects of wind over noise propagation the reader is referred to [25].

The aerodynamic and engine characteristics, all of them have been modeled using the Base of Aircraft Data (BADA) v4 Aircraft Performance Model (APM). BADA is an APM created and maintained by EUROCONTROL in cooperation with aircraft manufacturers and operating airlines [26], which includes performance data, aircraft operational and structural limits, needed to compute aircraft trajectories with enough accuracy to satisfy the requirements of new ATM systems.

CHAPTER 3. DESCENT TRAJECTORY OPTIMIZATION

As a brief introduction, the optimization of an aircraft trajectory can be formulated as a multi-phase constrained optimal control problem, where a cost function (J) is maximized or minimized by means of determining the controls of a system while satisfying a set of constraints. These types of problems are non-feasible from an analytical point of view, as their composition is based on complex non-linear functions. Thus, in order to solve them in a numerical way, a discretization approach is presented. This being said, in this chapter, the methodology proposed to solve this optimization problem will be exposed. Although the implementation exposed here would be valid for the optimization of both; departure and arrival procedures, only different arrival scenarios will be finally studied.

3.1. Optimal control problem formulation

In line with the control theory formulation, time $t \in \mathbb{R}$ is introduced as the independent variable for this problem, where it is defined within a given time interval $[t_0, t_f] \subset \mathbb{R}$, where t_0 and t_f are, respectively, the initial and final time values of the optimal trajectory. Although t_f is not fixed during the optimization, as it is the decision variable that must be taken into account during the optimization. Then, let the state vector, describing the trajectory of the aircraft over time, be $\vec{x}(t) \in \mathbb{R}^{n_x}$. $\vec{u}(t) \in \mathbb{R}^{n_u}$ the vector of time-dependent control variables which lead to a specific trajectory. Thus, the set of decision variables defining an optimal flight trajectory are determined by $\vec{z}(t) = [\vec{x}(t), \vec{u}(t), t_f]^T$.

In addition, accordingly, with the aircraft dynamics equations defined in section 2.3., the state vector can be described as:

$$\vec{x}(t) = \begin{bmatrix} v(t) & \chi(t) & n(t) & e(t) & h_p(t) \end{bmatrix}^T \tag{3.1}$$

Where $v(t)$ is the true airspeed (TAS); $\chi(t)$ is the aerodynamic heading angle; and $n(t)$, $e(t)$, $h_p(t)$ are respectively the northward, eastward and height coordinates, describing the position of the aicraft center mass.

In addition, the control vector is defined as:

$$\vec{u}(t) = \begin{bmatrix} \gamma(t) & \mu(t) & T(t) \end{bmatrix}^T \tag{3.2}$$

where $\gamma(t)$ is the aerodynamic path angle, $\mu(t)$ is the aerodynamic bank angle and $T(t)$ is the aircraft thrust.

3.1.1. Optimization criteria

In order to optimize a given trajectory, it is required to introduce a scalar index J, also known as cost criterion or cost value, which by means of a conveniently defined cost function, quantifies the achievement of the imposed objective. Being the cost function defined.

the optimization process can then be implemented as the mathematical minimization, or maximization, of such cost value, which depends on the vector of decision variables.

Furthermore, depending on the number of cost functions defining the optimization, the problem can be classified as single-objective if an individual cost value is implemented, or a multi-objective optimization problem, when two or more objective functions J_i are defined. In the majority of cases, when a multi-objective optimization problem is being solved, the different objectives are in conflict, in other words, a better performance in some optimization criterion J_x can lead to a worse performance in J_y. Thus, a trade-off rule between objectives must be meticulously assessed.

As in this project, the optimization of noise abatement procedures is being tackled, the final goal is to find the best trajectory $\vec{z}(t)$ that minimizes a set of n_J objectives defining the annoyance impact and ATM considerations:

$$\min_{\vec{z}} \{J_1(\vec{z}), J_2(\vec{z}), ..., J_{n_J}(\vec{z})\} \tag{3.3}$$

Details on the different cost criteria J_i and the interaction between them will be given in chapter 4.

3.1.2. Optimization contraints

To obtain a feasible and realistic trajectory, a set of constraints must be defined. In concordance with the process described before, the constraints defining the set of feasible trajectories can be grouped into four types; dynamic constraints, event constraint, path constraints and box constraints. Also, before proceeding it is worth mentioning, that the trajectory subject to optimization, will be divided into a number N of flight phases i, where each phase has a different aircraft configuration, as well as, different constraints imposed.

This said, firstly, *dynamic constraints* are those which describe the dynamics of the aircraft and can be defined as follows:

$$\frac{d\vec{x}^{(i)}}{dt} = \dot{\vec{x}}^{(i)}(t) = f^{(i)}(\vec{x}^{(i)}(t), \vec{u}^{(i)}(t)) \quad i \in [1, N] \tag{3.4}$$

where function $f : \mathbb{R}^{n_x+n_u} \rightarrow \mathbb{R}^{n_x}$ is the non-linear function presented in equation 2.16.

Secondly, *event constraints* are those fixing the initial and final boundary conditions:

$$\vec{\eta}_L^{(i)} \leq \vec{\eta}^{(i)}(\vec{x}^{(i)}(t_0), \vec{x}^{(i)}(t_f), t_0^{(i)}, t_f^{(i)}) \leq \vec{\eta}_U^{(i)} \quad i \in [1, N] \tag{3.5}$$

where function $\vec{\eta} : \mathbb{R}^{2(n_x+1)} \rightarrow \mathbb{R}^{n_\eta}$ describes the n_η different event constraints and $\vec{x}_U$ and $\vec{x}_L$ are, respectively, the corresponding upper and lower bounds. In the scenario proposed, even constraints are divided on those defining the trigger condition between phases, which will be explained later in the profile definition, and those defining the initial and final conditions of the trajectory (Boundary conditions) which in this case are:

$$\begin{aligned}
h^{(1)}(t_0) &= h_{cruise} & v_{CAS}^{(N)}(t_f) &= v_{CAS,ILS} \\
M^{(1)}(t_0) &= M_{cruise} & \chi^{(N)}(t_f) &= \chi_{RWY} \\
t^{(1)}(t_0) &= 0 & h^{(N)}(t_f) &= h_{ILS} \\
n^{(1)}(t_0) &= n_0 & n^{(N)}(t_f) &= n_{ILS} \\
e^{(1)}(t_0) &= e_0 & e^{(N)}(t_f) &= e_{ILS}
\end{aligned} \tag{3.6}$$

where h_{cruise}, M_{cruise}, n_0 and e_0 are respectively the imposed cruise altitude, mach speed and north-east coordinates which will be defining the starting point ($t^{(1)}(t_0) = 0$) of the trajectory; χ_{RWY} is the runway heading angle; h_{ILS} is the imposed height at which the aircraft will be intercepting the ILS and as a concequence, the coordinates n_{ILS} and e_{ILS} with the Calibrated Airspeed (CAS) v_{ILS} is also fixed.

On third place, path constraints restrict the beahaviour of some variables all along a given phase i:

$$\vec{\psi}_L^{(i)} \leq \vec{\psi}^{(i)}(\vec{x}^{(i)}(t), \vec{u}^{(i)}, t) \leq \vec{\psi}_U^{(i)} \quad i \in [1, N] \tag{3.7}$$

As similarly found in event constraints, function $\vec{\psi} : \mathbb{R}^{n_x+n_u+1} \rightarrow \mathbb{R}^{n_\psi}$ defines the n_ψ different path constraints and $\vec{\psi}_U$ and $\vec{\psi}_L$ are the upper and lower bounds, respectively. Later, the aircraft profile will be explained where multiple examples of path constraints may be found.

Last but not least, box constraints bound the state and control variables during the trajectory optimization:

$$\begin{aligned}
\vec{x}_L^{(i)} &\leq \vec{x}^{(i)} \leq \vec{x}_U^{(i)} \\
\vec{u}_L^{(i)} &\leq \vec{u}^{(i)} \leq \vec{u}_U^{(i)}
\end{aligned} \qquad i \in [1, N] \tag{3.8}$$

where $\vec{x}_L \in \mathbb{R}^{n_x}$, $\vec{x}_U \in \mathbb{R}^{n_x}$, $\vec{u}_L \in \mathbb{R}^{n_u}$ and $\vec{u}_U \in \mathbb{R}^{n_u}$ are the Lower and Upper values bounding all control and state variables, which in our case will be defined by:

$$\begin{aligned}
&\gamma_{min} \leq \gamma^{(i)} \leq 0 \\
&\mu_{min} \leq \mu^{(i)} \leq \mu_{max} \qquad\qquad i \in [1, N] \\
&T_{min}(\vec{x}) \leq T^{(i)} \leq T_{max}(\vec{x})
\end{aligned} \tag{3.9}$$

being γ_{min} the minimum flight path angle corresponding tot he minimum descent gradient; μ_{min} and μ_{max} the bank angle operational bounds; and $T_{min}(\vec{x})$ and $T_{max}(\vec{x})$ are the minimum and maximum thrust, respectively, both of them, functions of the temperature, pressure and Mach number.

3.1.2.1. Profile

In order to define a trajectory suitable to meet the requirements imposed by actual ATM systems, a proper profile is defined where the descent trajectory is divided in a set of different phases. Each of them containing specific constraints to meet not only airspace regulations but aircraft operational limitations. Table 3.1.2.1. shows all the path and event

constraints imposed during the descent. Those constraints can be found defined in terms of the match number M, the calibrated airspeed v_{CAS}, the pressure altitude h_p, the aircraft thrust T, the aerodynamic path angle γ and the energy share factor k. Although it is not included in the table, the aerodynamic path angle has been bounded to a minimum value of $-7°$ for all the phases going from the Cruise (1) to the Clean Approach (6).

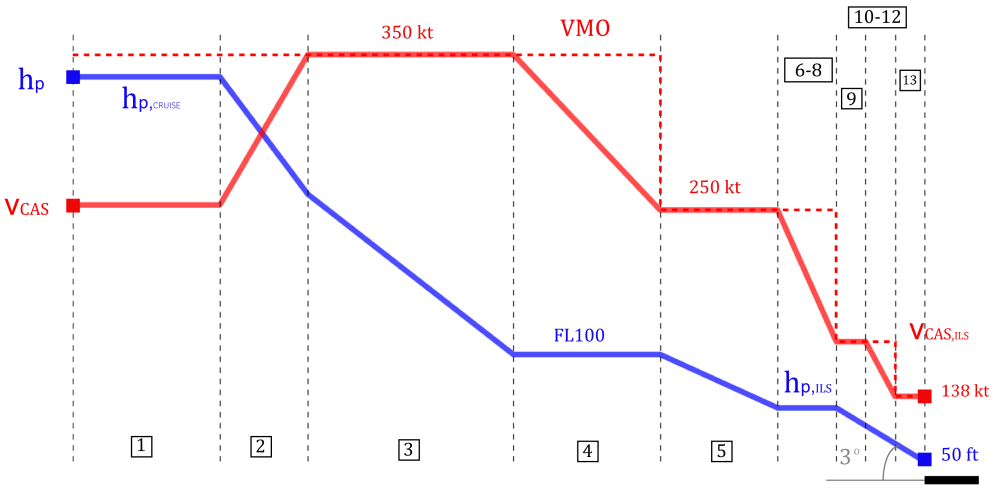

Figure 3.1: h_p and v_{cas} vertical profiles

In addition, Figure 3.1, gives a better visualization of the pressure altitude and calibrated airspeed profiles. Notice, that although being an idle Thrust continue descent profile, there are two constant altitude phases imposed, which give a better adjustment of the trajectory to realistic ATM scenarios. As an example, the second level-off phase, performed at $h_{p,ILS}$ altitude, enables an easier interception of the ILS.

3.1.3. Problem resolution

Once the problem is conveniently defined, there exist several methodologies which could be implemented in order to solve it. As mentioned in section 1.2.2.3., analytical methods are infeasible due to the existing non-linearities defining the problem and the difficulty to determine the sequence of constrained arcs. Thus, numerical methods are chosen as the unique feasible alternative.

In this project, in concordance with past work done within the research team [16, 14, 15], direct collocation methods are chosen due to the fact that such methodology can easily cope with inequality constraints without implying a high computational burden.

Direct collocation methods transform the original continuous optimal control problem into a discrete and finite Non-linear Programming (NLP) optimization problem. This is done by means of discretizing time histories of control and state variables into a set of collocation points, which values become the unknowns of the new finite variable problem, effectively reducing the problem to an NLP that can be solved by a standard non-linear programming code.

Within the multiple collocation schemes available, the trapezoidal collocation method is

ID	Phase	Event constraints (η)	Path constraints (ψ)
1	Cruise	$M(t_0) = 0.78$ $n(t_0) = n_0; e(t_0) = e_0$ $t(t_0) = 0$	$h_p = 36{,}000$ ft $\dot{M} = 0$
2	Descent Mach	$h(t_0) = 36{,}000$ ft	$T = T_{idle}$ $M \leq MMO; \dot{M} = 0$
3	Descent CAS	$M(t_0) = 0.78$	$200 \text{ kt} \leq v_{CAS} \leq VMO$ $T = T_{idle}; \dot{v}_{CAS} = 0$
4	Descent deceleration	$v_{CAS}(t_0) = 300$ kt	$200 \text{ kt} \leq v_{CAS} \leq VMO$ $T = T_{idle}; \dot{k} = 0$
5	Approach CAS	$h(t_0) = 10{,}000$ ft	$200 \text{ kt} \leq v_{CAS} \leq VMO$ $T = T_{idle}$
6	Approach Clean	$v_{CAS}(t_0) = 250$ kt	$200 \text{ kt} \leq v_{CAS} \leq 250$ kt $\dot{k} = 0; T = T_{idle}$
7	Final	$200 \text{ kt} \leq v_{CAS}(t_0) \leq 210$ kt	$190 \text{ kt} \leq v_{CAS} \leq 210$ kt; $\dot{k} = 0$ $0^\circ \geq \gamma \geq -3^\circ$; $T = T_{idle}$
8	Config 2 - Glide Slope Up	$160 \text{ kt} \leq v_{CAS}(t_0) \leq 200$ kt	$T = T_{idle}$ $\dot{h} = 0$
9	FAP	$h(t_0) = h_{ILS}$	$v_{CAS} = v_{CAS,ILS}$ $\gamma = -3^\circ$
10	Config 2 - Glide Slope Down	$v_{CAS(t_0)} = v_{CAS,ILS}$	$\gamma = -3^\circ$
11	Config 3 - Glide Slope	$v_{CAS(t_0)} = 155$ kt	$\gamma = -3^\circ$
12	Full Glide Slope	$v_{CAS(t_0)} = 148$ kt	$\gamma = -3^\circ$
13	Glide Slope stab	$h(t_0) = 1000$ ft; $h(t_f) = 50$ ft; $n(t_f) = n_{RWY}; e(t_f) = e_{RWY}$ $v_{CAS(t_f)} = 138$ kt	$\gamma = -3^\circ$ $v_{CAS} = 138$ kt

Table 3.1: Vertical flight profile

selected as its less expensive computational cost and accuracy offer a good suit for the problem resolution. For more information on the mathematical formulation of optimal control problems for the optimization of aircraft trajectories, see [16].

3.2. Software Implementation

The optimization engine of this project relies on DYNAMO (DYNAMic Optimiser) [6], a trajectory optimization framework developed at the Technical University of Catalonia, capable of computing 4D trajectories in different contexts. DYNAMO offers great flexibility allowing for an easy implementation of different flight profiles and scenarios, going from completely unconstrained continuous operations, to defined standard procedures such as standard instrument departures and arrivals (SID, STAR), or, in this case, noise abatement departure procedures, etc.

For this project, some new features have been added to the aformentioned framework with the aim of tailoring the software to the project needs. The main contribution has been made on the dynamics block, which has been expanded in order to enable the optimization of aircraft trajectories not only on the vertical plane but also in the lateral one. Also, all the required changes have been conducted with the porpuse of implementing the noise model defined in section 2.1..

Figure 3.2 shows the basic workflow of the implemented trajectory optimization environment. As it can be seen in the diagram, four different files describe the scenario set to

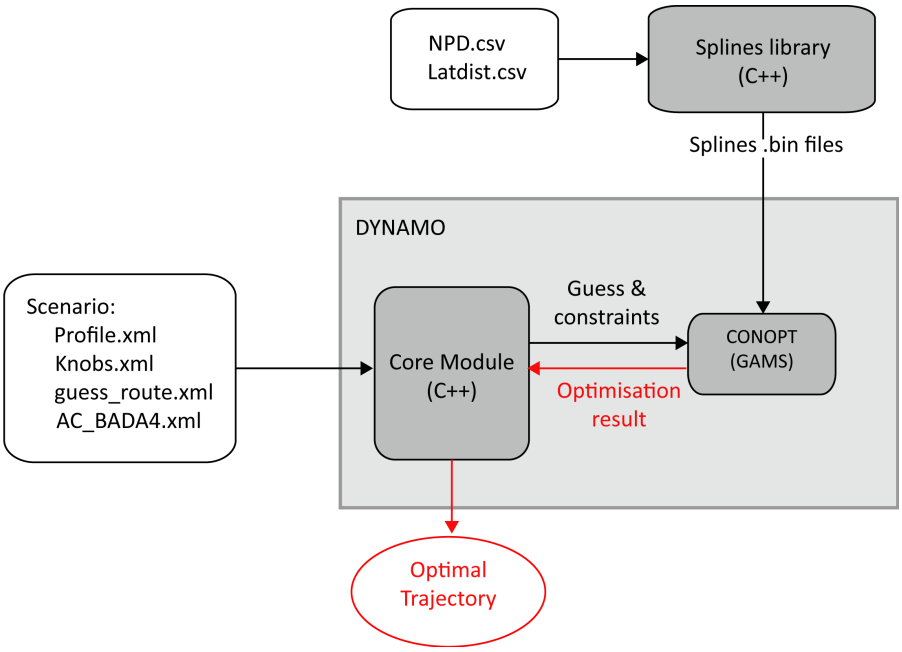

Figure 3.2: Implemented Software Diagram

optimize the descent trajectory. First, the profile .xml file describes the vertical profile constraints introduced on section 3.1.2.1., and it is used to define the guess variables describing the vertical trajectory. On the other hand, the guess_route.xml file contains the set of points defining the lateral route to be taken into account for the guess profile. In third place, the knobs file contains all the tuning options available on the DYNAMO framework, options such as the cost function to be minimized, the collocation method, the meteorology model, etc. Finally, the BADA4 xml file contains all the performance information for a given aircraft model. For more information about the information contained in those files and where to find them see [26].

All those files defining the scenario, are introduced as inputs to the main core module of the framework, which is coded in C++ and generates all the required variables and parameters defining the guess, and all the constraints needed by the optimizer to solve the problem. It is worth mentioning that NLP solvers need an initial trajectory from which the iteration process towards the solution starts. This initial trajectory, which does not need to be optimal, or even feasible, is called guess.In this module, all the dynamics, performance and weather models are implemented in order to produce the initial guess according to ATM systems simulation standards.

3.2.1. The CONOPT solver

As mentioned in section 3.1.3., the optimal control problem formulated will be solved using trapezoidal direct collocation methods, which transform the original continuous OCP into an NLP optimization problem. Then, it can be solved using large-scale efficient and reliable solvers bundled into the General Algebraic Modelling System (GAMS) software suite.

For this project, the CONOPT module has been chosen between all the available solvers included in the GAMS optimization package, as it has successfully proved to be an effi-

cient package to solve large problems with thousands of variables and constraints, and highly non-linear functions. Its optimization algorithm starts by finding a feasible solution, following by a two-phase iterative procedure, which consists of [5]:

- Finding a search direction, through the use of the Jacobian of the constraints, the selection of a set of basic variables and the computation of the reduced gradient.
- Performing a search in this direction, though a pseudo-Newton process until a convergence criterion is met.

However, the CONOPT solver is aimed at solving generic NLP problems, as mentioned in section 1.2.2.3.,for those kind of problems it is not possible to check, once the algorithm has ended, if the solution satisfies the optimal first-order necessary conditions. Thus, the obtained solution will be, in general locally optimal, which is a strong point to bear in mind.

This being said, once the optimizer has ended, the solution will be sent again to the DYNAMO core module, which will process the results and export them in a .dat file.

3.2.2. Splines implementation

As mentioned in section 2.1. both surfaces; $L_{max}(P,d)$ and $l_{NSA}(n,e)$, are approximated as mathematical functions defined by spline fitting methods. Splines are functions defined piece-wise by polynomials of any degree, which keep a sufficiently high grade of smoothness at the places where the polynomial pieces connect, also called knots. For more information on splines mathematical theory see [27].

Concerning the aircraft descent trajectory optimization, the main advantage of splines is that they are continuous and differentiable even if defined as a piece-wise function, which is a requirement when using NLP for the optimization problem resolution [28]. Also, spline

```
#include <iostream>
#include <splineutilities.h>

int main(){

const std::string dir = "../NPDs/";
const std::string filename = "A320-232_LAmax_A_40dB.csv";
const std::string outfile = "../NPDs/A320-232_LAmax_A_40.bin";

fitpackpp::BSplineSurface *ptr = new fitpackpp::BSplineSurface;

double smoothing = 10;

generateSpline(&ptr, dir, outfile, filename, smoothing);

}
```

Figure 3.3: BSplineSurface C++ implementation

interpolation is usually preferred over polynomial interpolation, due to the fact that the error made when evaluating a certain data point can be small even when using low degree polynomials for the spline definition.

This being said, in order to generate the splines, a library called Fitpackpp, which is a wrapper of the well-known Fortran library called FITPACK [29], has been used for this project. The library contains a ”BSplineSurface” class wrapping the 2D routines ”surfit”, ”bispev”, and ”parder”. Concretely, the routine ”surfit” has been selected, as it finds a spline representation of a surface, given a set of data points $(\vec{x},\vec{y},\vec{z})$ and a non-negative smoothing factor.

Figure 3.3, shows the actual implementation of the $L_{max}(P,d)$ surface spline. As it can be seen in the figure, a CSV file and the smoothing factor are entered as input, later, the function outputs a binary file containing the resulting spline parameters (control points, knots and degree). This binary file is opened in the GAMS model as a mathematical function. The value of the smoothing factor chosen during the process will be discussed in the next section.

CHAPTER 4. RESULTS

Throughout this section, all the results obtained along this project, regarding the descent trajectory optimization accordingly to the criteria exposed in section 3.1., will be exposed. Two main cases will be discussed with the aim of testing the performance of the proposed method. In the first section, the scenario implemented will be described. Later, in the second section, the implementation of the different cost criteria will be explained. Then, the obtained trajectories for both cases will be plotted in the north-east coordinates space, as well as the noise print showing the impact of the resulting descent procedure. Finally, different variables defining the obtained trajectory will be plotted in order to obtain relevant conclusions.

4.1. Scenario

With the aim of testing the methodology exposed in this project, a specific scenario will be defined, for which different results will be obtained and as a consequence, the corresponding conclusions will be established.

Concretely, the arrival route for the Barcelona-El Prat airport (LEBL) runway 07L will be used for this study. Also, all the different phases going from the cruise to the ILS interception point will be optimized. The interception point will be defined by means of the interception altitude, three different values (1.000, 2.000 and 3.000 ft) will be imposed in order to obtain three different trajectories. On the other hand, the initial point will be set to be at the NW of the airport, with the aim of avoiding sea areas and obtain a clearer picture of the embraced methodology.

This being said, the aircraft model chosen for this experiment will be the Airbus A320-232, which is one of the most common aircraft currently operating in this airport. The performance file has been obtained from the BADA4 dataset and also the corresponding $L_{max}(P,d)$ curve in arrival configuration and with a 40 dB(A) imposed threshold, has been computed in order to meet the optimization requirements.

The vertical trajectory will be defined and constrained following exactly the same vertical

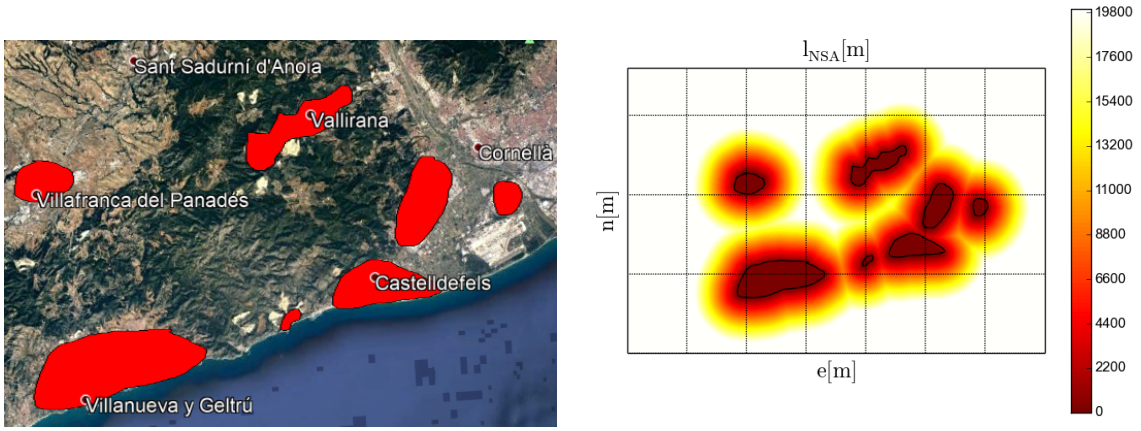

(a) NSAs definition

(b) $l_{NSA}(n,e)$ surface

Figure 4.1: Scenario NSAs definition and contour plot

profile described in section 3.1.2.1., where the distance to the runway (x) at the FAP phase will be imposed accordingly to the aforementioned interception height.

Regarding the definition of the noise sensitive areas, an approximate selection of the most affected urban centers has been made. It is important to clarify that modeling the most affected zones by the 07L landing procedure is out of the scope of this project, due to the complexity and the political decisions interfering in the selection process. This being said, the proposed scenario serves just as a proof of concept. Figure 4.1(a), shows the selection of the different NSAs which has been made using the Google Earth software, the resulting kml files defining the different contours have been processed using a python script which computes the final $l_{NSA}(n,e)$ curve into a CSV file, following the algorithm explained in section 2.2.1. (see Figure 4.1(b)).

As explained in the last section, both the $L_{max}(P,d)$ and $l_{NSA}(n,e)$ surfaces are introduced to the CONOPT optimizer as mathematical functions defined by splines. This is achieved by means of a C++ module which gets as inputs the three vectors defining the surface and a non-negative smoothing factor. The election of a smooth factor is often tricky as there is no certain way of defining which value suits better the needs of the optimizer while defining properly the surface shape. As an example, due to the simplicity of the $L_{max}(P,d)$ curve, a smooth factor of 10 has been selected, which it can be considered to be large in comparison to the 0.01 value chosen for $l_{NSA}(n,e)$ surface, which is far more complex in its shape. In the next chapter, the results will be used to show which indications have been used to see if the splines functions smoothing factors are properly defined.

Finally, the current scenario will be tested using mainly two different implementations which will be divided in two different cases. Each case will present different cost criteria dealing with the minimization of the noise impact produced by each arrival trajectory. Thus, the different objective functions definitions and the results comparing, the different performances of the optimizer will be exposed in the following sections.

4.2. Cost function definition

As explained in section 1.2.2., there are several approaches dealing with the definition of the most convenient objective function for optimizing NAPs. Defining a specific cost function may imply reducing the annoyance in some areas and consequently aggravate the impact on others. Thus, as there exists a set of subjective decisions, the responsibility of embracing one approach commonly relapses over regulators and government entities.

As a first approach, our optimization problem has been set to minimize just one objective J, which addresses the whole annoyance impact of the trajectory, integrating in time the maximum Noise level perceived at the closest NSA border point (L_{max}) for every instant of time t. Also, with the aim of only taking into account the perceived noise levels over the imposed threshold value, the L^*_{max} has been subtracted for every noise level obtained for different time instants. In addition, as the aircraft trajectory is divided in a number N of phases, the contribution of each phase i has been added together, defining, thus, the final annoyance cost function associated to the aircraft trajectory as:

$$J = \sum_{i=1}^{N} \int_{t_0^{(i)}}^{t_f^{(i)}} \left(L_{max}(\vec{x}^{(i)}(t), \vec{u}^{(i)}(t)) - L^*_{max} \right) \, \mathrm{d}t \tag{4.1}$$

where L_{max} is the computed LAMAX level at the closest NSA point and L^*_{max} is the noise threshold value imposed during the optimization (in this case, the ambient noise).

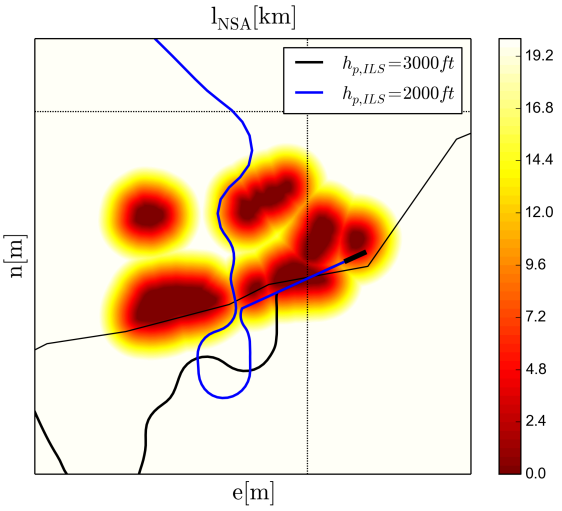

Figure 4.2: First results for noise minimization

However, a new problem arises when implementing the aforementioned cost function. As figure 4.2 shows, although being completely feasible from the annoyance reduction point of view, the obtained trajectories take unrealistic paths which do not seem feasible for a realistic ATM scenario. The main reason behind this type of response is the ambiguity generated by the cost function, which only takes into account the annoyance over the threshold, and as a consequence, the optimizer finds a lot of points on the trajectory where is able to find more than one feasible solution without changing the cost value.

With the aim of solving this problem, the time duration of the trajectory will be introduced as a second objective which will constraint the problem to such an extent where just one solution can be found. As explained, in section 3.1.1., when implementing multiple objective functions conflicting which each other, a set of rules determining the trade-off between objectives must be defined.

For this reason, in the next two sections, two different methods will be presented in two different cases, each one of them taking different approaches in order to tackle the problem.

4.2.1. Case 1: Lexicographic optimization

The first approach implements what is called a lexicographic optimization, which establishes a hierarchical order among all the optimization objectives, going from the most important J_1 to the least important J_{n_J} [1].

In first place, as minimizing the noise exposure is the main goal of the optimization, the cost function described in equation 4.2 will be minimized as the first objective J_1:

$$J_1 = \sum_{i=1}^{N} \int_{t_0^{(i)}}^{t_f^{(i)}} \left(L_{max}(\vec{x}^{(i)}(t), \vec{u}^{(i)}(t)) - L^*_{max} \right) \, \mathrm{d}t \tag{4.2}$$

Then, a second optimization will take place, where a second objective J_2 will be imposed with the aim of minimizing the whole duration of the trajectory:

$$J_2 = \sum_{i=1}^{i=N} \int_{t_0^{(i)}}^{t_f^{(i)}} \mathrm{d}t \tag{4.3}$$

where the second optimization problem minimizing the flight time, will be limited by a new constraint forcing to fulfill the first objective index obtained during the noise optimization.

$$J_1 \leq J_1^* \tag{4.4}$$

where J_1^* is the obtained cost function value of the previous optimization (see equation 4.2).

4.2.2. Case 2: Weighted optimization

For the second approach just one objective function J will be defined, where a noise index NI will be introduced with the aim of quantifying the trade-off between noise impact and time. The higher the noise index, the more importance to reduce the flight time will be given by the trajectory and viceversa. Thus, the cost function J can be defined as:

$$J = \sum_{i=1}^{i=N} \int_{t_0^{(i)}}^{t_f^{(i)}} \left(L_{max}(\vec{x}^{(i)}(t), \vec{u}^{(i)}(t)) - L_{max}^* + NI \right) \mathrm{d}t \tag{4.5}$$

where NI is the noise index which units are dB(A)/s.

4.3. Optimization results

In this section, the different results obtained for the two aforementioned cases will be presented. For each case, three ILS interception altitudes (1000, 2000 and 3000 ft) have been imposed with the aim of providing a better intuition on the optimizer performance. The trajectories obtained have been projected in the l_{NSA} contour plot, which defines the lateral distance to the closest NSA point for every pair of coordinates north-east.

In addition, six different plots, exposing the most relevant variables defining the states, controls, and the cost function value obtained will be exposed as well as noise footprints exhibiting the noise impact of the obtained trajectories on the pre-defined noise sensitive areas.

4.3.1. Case 1: Lexicographic optimization

Regarding the first case, figure 4.3 shows the results obtained when minimizing the noise impact of the trajectory as a whole, following the algorithm defined in section 4.2.1.. As it can be seen in the figure, three different results are obtained for the different interception altitudes imposing a noise threshold L_{max}^* of 40 dB. The reader may take into account, that

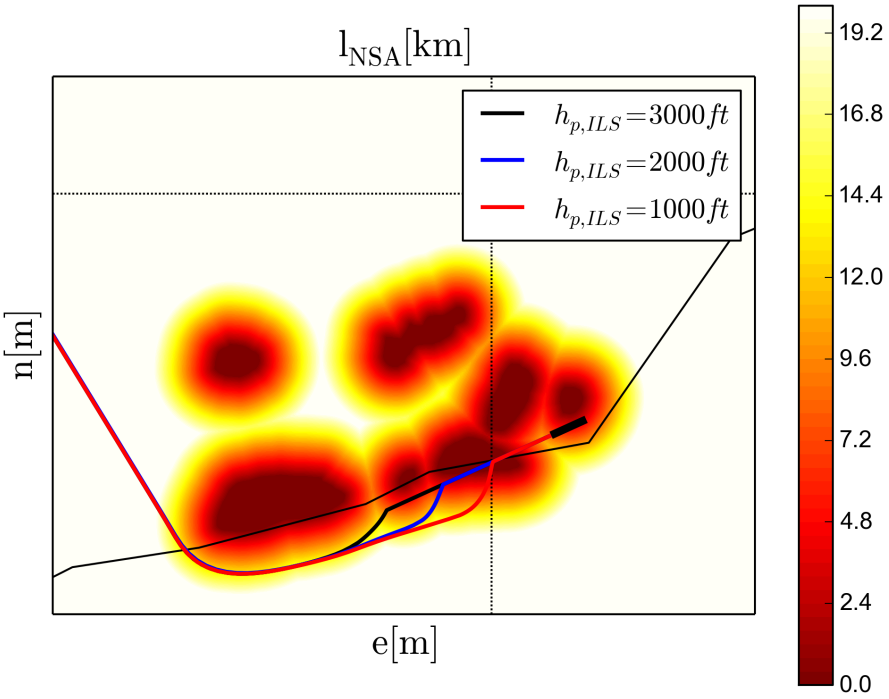

Figure 4.3: Case 1 flight tracks

the cost values J_1^* obtained for the 2000 and 3000 ft interception altitudes are the same that the obtained for the trajectories exposed in figure 4.2, which reflects how different can be two given trajectories with the same cost value, when the problem is not completely bound.

In addition, the exposed results show how adding the time variable to the optimization closes the problem obtaining three trajectories which could be feasible from an ATM system point of view. As noise impact reduction is the main goal, being the first in the hierarchical list, the obtained trajectories avoid as much as possible all the defined NSAs.

Furthermore, in figure 4.4, different variables defining the resulting trajectories can be found plotted as a function of the distance x to the runway. Starting with the pressure altitude h_p (see figure 4.4(a)), it can be seen how the trajectory follows the profile described in section 3.1.2.1., and how the ILS is intercepted at the three different imposed altitudes. In addition, figure 4.4(b) shows how the results follow as well the imposed speed profile, notice how each solution starts the deceleration at different points of the trajectory and how once the ILS is intercepted all of them follow the same profile.

On the other hand, figure 4.4(c) and 4.4(d), show how the controls perform during the three different descents. The flight path angle plot shows how all the values lie over the -7° imposed constraint, and how all the three lines end with the ILS -3° descent. Regarding the throttle, the figure exposes how almost all the descent is performed at idle Thrust, until a point where some thrust power is used to maintain the enforced flight path angle in the ILS glide path and the final approach speed.

slow down the airplane before the touchdown.

Finally, the last two plots, show the noise impact of the obtained trajectories on the ”measurement grid”. Figure 4.4(f), shows the L_{max} level under the flight track, without taking

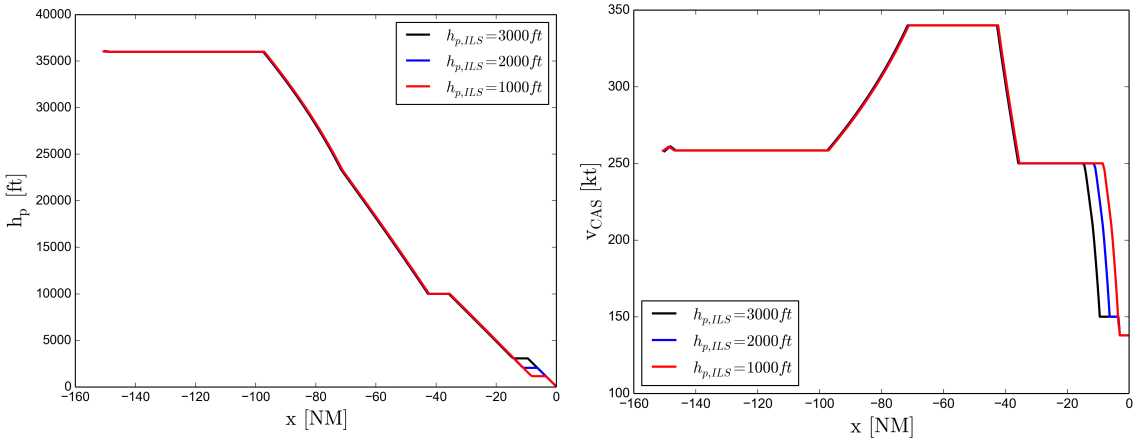

(a) Pressure altitude h_p

(b) Calibrated air speed v_{CAS}

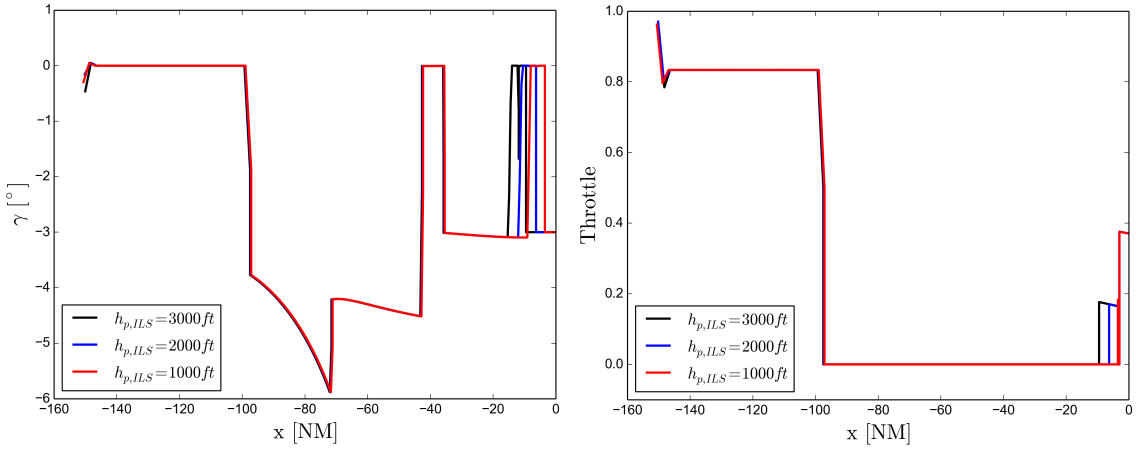

(c) Flight path angle γ

(d) Throttle

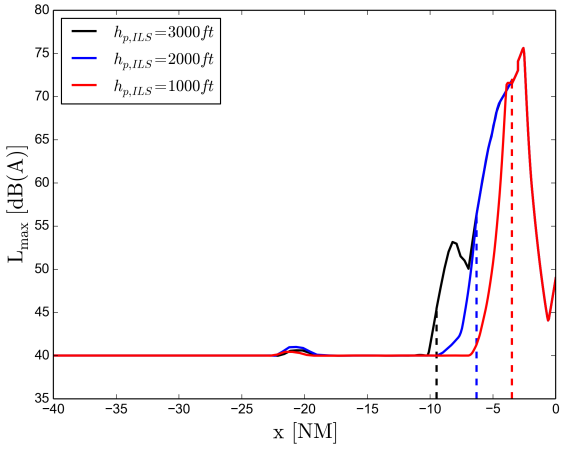

(e) L_{max} noise level at the closest NSA

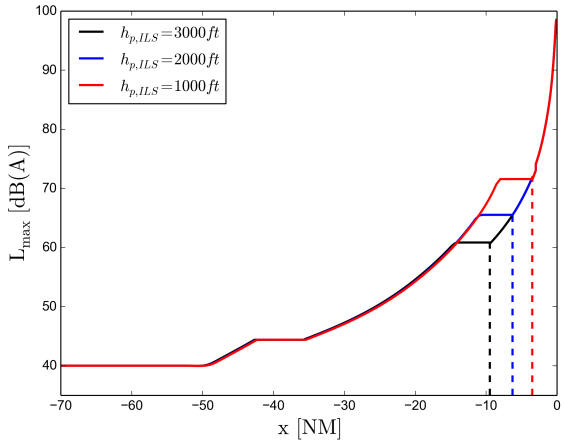

(f) L_{max} noise level under the flight track

Figure 4.4: Case 1 plots

into account the different NSAs. On the contrary, figure 4.4(e) shows the L_{max} level computed at the closest NSA border point. At a first glance, it can be seen how the 40 dB(A) threshold is respected as a straight line and without presenting smaller values, which is one of the indicatives used to verify the correct implementation of the splines functions.

In addition, it is important to notice how the noise under the flight track is maintained lower during the last phases of the descent when the interception of the ILS is performed earlier, which would be a good measure to implement for arrivals where the lateral route is fixed. However, the L_{max} level at the NSAs shows how the late interception of the ILS, gives the aircraft more freedom to take lateral maneuvers in order to avoid the NSAs and, thus, decreasing the noise impact. Also, it is important to notice how all the perceived noise levels are equal once each of the trajectories intercepts the ILS.

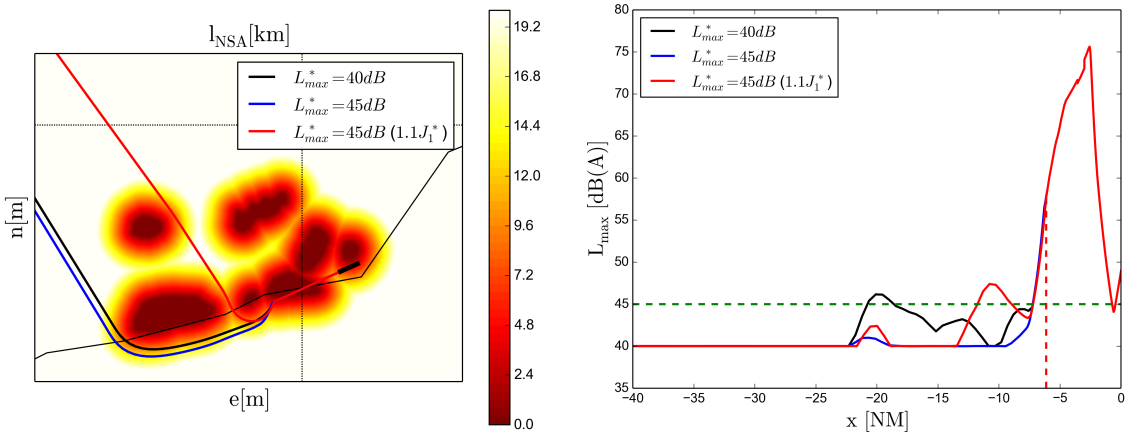

(a) Results flight tracks

(b) L_{max} noise level at the closest NSA

Figure 4.5: Trajectory results for relaxed L^*_{max} and J^*_1 values

To conclude, some tests were conducted, in order to see the optimizer performance when changing the noise threshold and relaxing the J^*_1 value in order to allow less restrictive trajectories. Figure 4.5 shows the results obtained for a 2000 ft ILS interception altitude, where two new cases are exposed and compared to the result obtained in the last case. As it can be seen in figure 4.5(a), a slight difference can be appreciated when relaxing the noise threshold to 45 dB(A). However, for the same configuration if the cost value J^*_1 obtained for the first noise optimization is relaxed a 10%, the solution is drastically different. In addition, figure 4.5(b), shows the obtained noise level at the closest NSA border point, processed with a noise threshold of 40 dB(A) in order to give a better clarity of comparison. It is important to notice, the subtle 10% difference between the red line and the blue one, and how drastic the difference in the trajectory is. It seems clear how imposing different noise thresholds with different J^*_1 relaxed values opens new possibilities in trajectories where the time of arrival must be taken into account.

4.3.2. Case 2: Weighted optimization

For the second case, figure 4.6 shows the results obtained when minimizing the noise impact of the trajectory as a whole, following the cost function defined in section 4.2.2.. As it can be seen in the image, three drastically different results are obtained for the different

interception altitudes imposing a noise threshold L^*_{max} of 40 dB(A) with a noise index NI of 40 dB(A)/s.

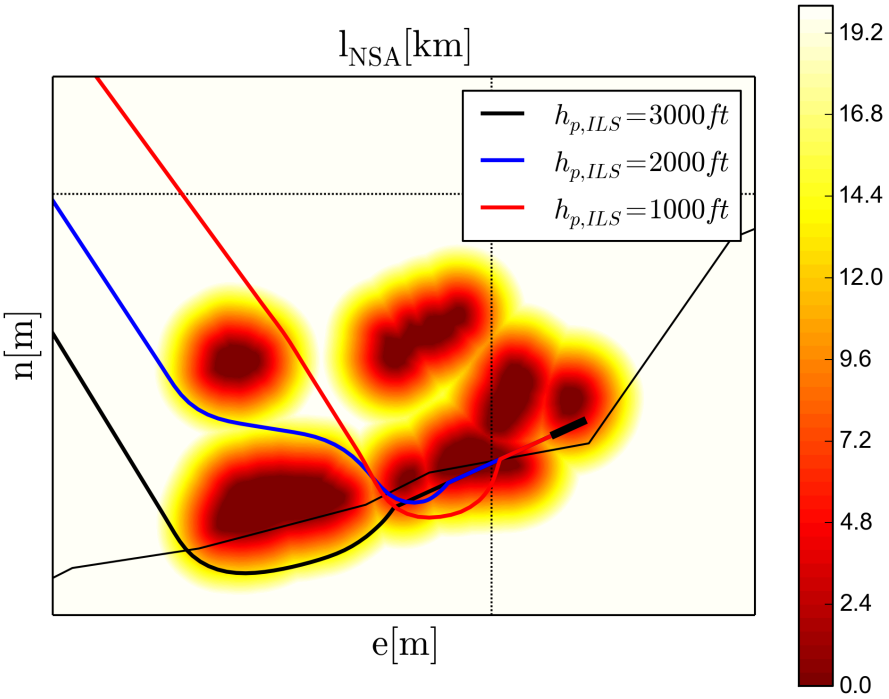

Figure 4.6: Case 2 flight trakcs results

The results show how taking into account both noise and time at the same time leads to a less restrictive operation of the descent trajectories, taking shortcuts in order to reduce the flight time. However, this induces an increase in the perceived L_{max} levels at the NSAs, which plot can be found in figure 4.7(e). In addition, the results show again how in this case, a late interception of the ILS allows the aircraft to take lateral maneuvers in order to avoid the NSAs at the end of the descent when the noise impact is at its worst.

Regarding the rest of the plots exposed in figure 4.7, similar performances, in comparison with the first case, can be found in both the h_p and v_{CAS} profiles, and again in the flight path angle γ and the throttle parameter.

To conclude, it is worth saying that, there are strong similarities in the concept defining this implementation and the example showed in the last section where the J^*_1 value was reduced a 10%. Adjusting the value of the parameter NI and the relaxation of the obtained cost value J^*_1 might even lead to the same results, However, the implementation taken in case 2, offers a more simple solution and only needs to run the optimization process once. Nevertheless, the implementation of case 1 is useful in cases where it is desired to minimize noise at its maximum and then minimize time at the ”remaining space” left by the first optimization step.

4.4. Noise footprints

With the aim of proving the obtained results and providing a better visualization of the obtained trajectories, noise footprints of the two sets of three trajectories, obtained for the two

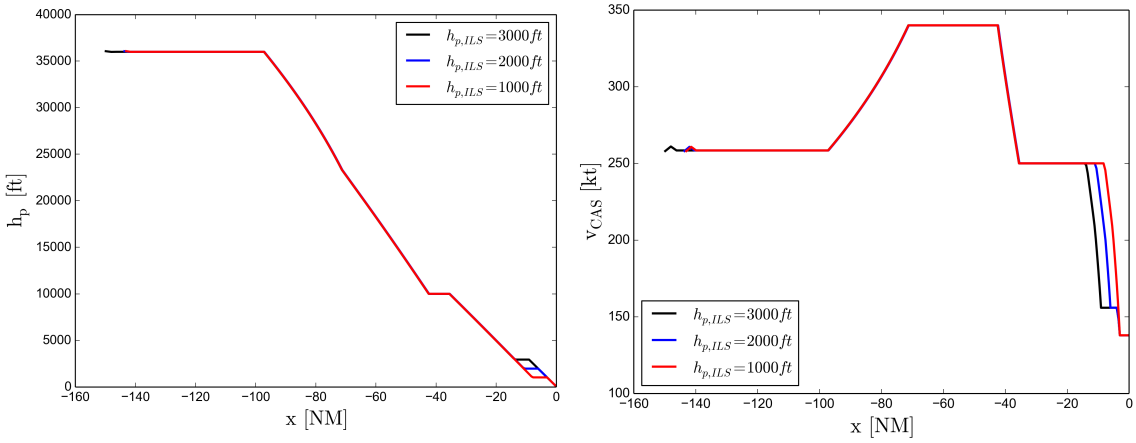

(a) Pressure altitude h_p

(b) Calibrated air speed v_{CAS}

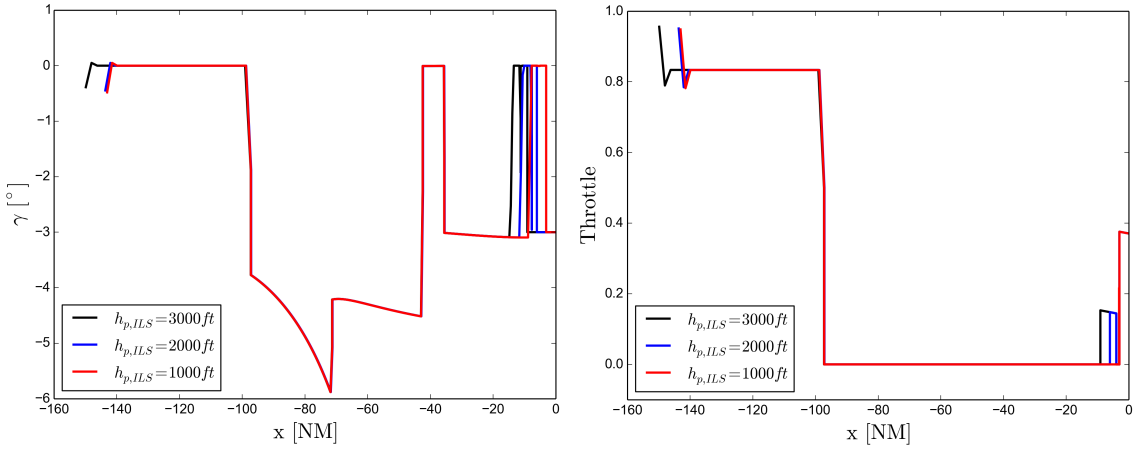

(c) Flight path angle γ

(d) Throttle

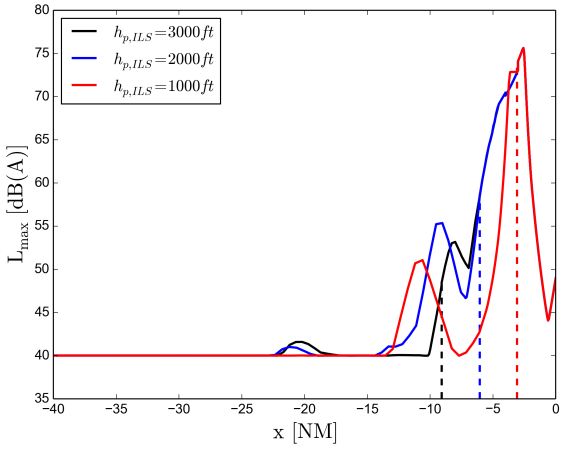

(e) L_{max} noise level at the closest NSA

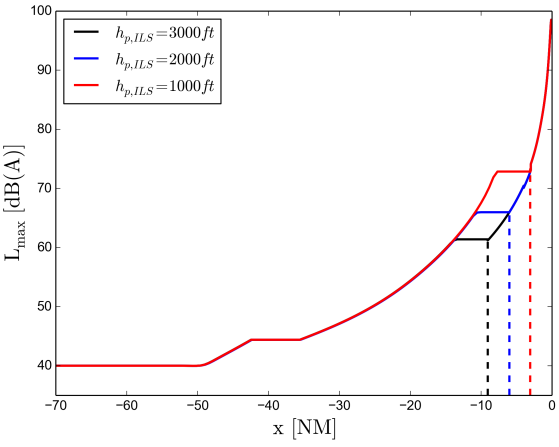

(f) L_{max} noise level under the flight track

Figure 4.7: Case 2 results plots

different cases, have been computed. The computation has been made implementing the noise model described in section 2.1., however, in this case, with the purpose of obtaining the most realistic representation of the emitted noise impact, the lateral attenuation factor has been taken into account. Thus, looking at the exposed noise footprints, our hypothesis where the worst case scenario was chosen, neglecting the lateral attenuation factor, may be verified.

Figures 4.9 and 4.8, show the noise prints, starting at 40 dB(A) and increasing 10 dB(A) for each contour area. Also, the different NSAs can be found plotted with red dotted lines, as well as the aircraft trajectory defined by the black line.

Looking at the figures in detail, it can be seen how both scenarios easily avoid the more distant NSAs, and as expected have some difficulties avoiding the NSAs located near the airport. Concretely, the reader may notice how the second set of results exposed in figure 4.9, have serious problems avoiding the small NSA located between the Castelldefels and the Vilanova areas, which can be a consequence of the imposed 40 dB(A)/s noise index NI or a local minimal found by the optimizer. However, for the first case implementation, as the interception altitude is set to lower values, the optimizer manages to reduce the noise impact under the threshold.

In addition, all the images show how the 70 dB(A) region is confined always in the last segment of the descent, once the ILS is intercepted. This reflects the limitation of optimized noise abatement procedures, as the most affected zone is restricted by the ILS descent segment, which is completely bounded by the constant 3° glide path, the speed profile imposed by the different flight configurations and the approach speed.

for safety reasons.

Finally, the noise footprints show how the results obtained are more conservative than needed, due to the no implementation of the lateral attenuation factor. As a result, in the three footprints exposed in figure 4.8, it can be seen how the lateral distance maintained to the NSA surrounding Vilanova does not follow exactly the NSA contour.

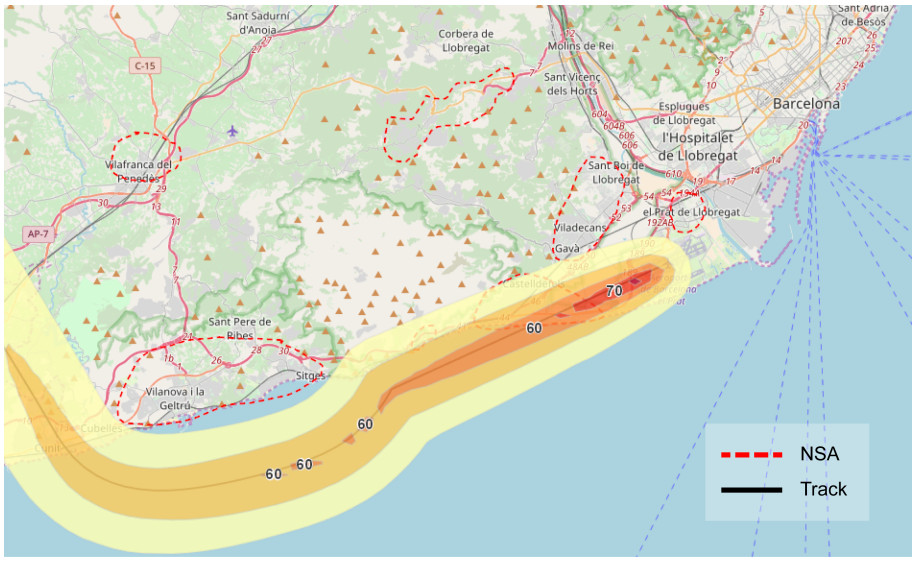

(a) h_{ILS} = 3000 ft

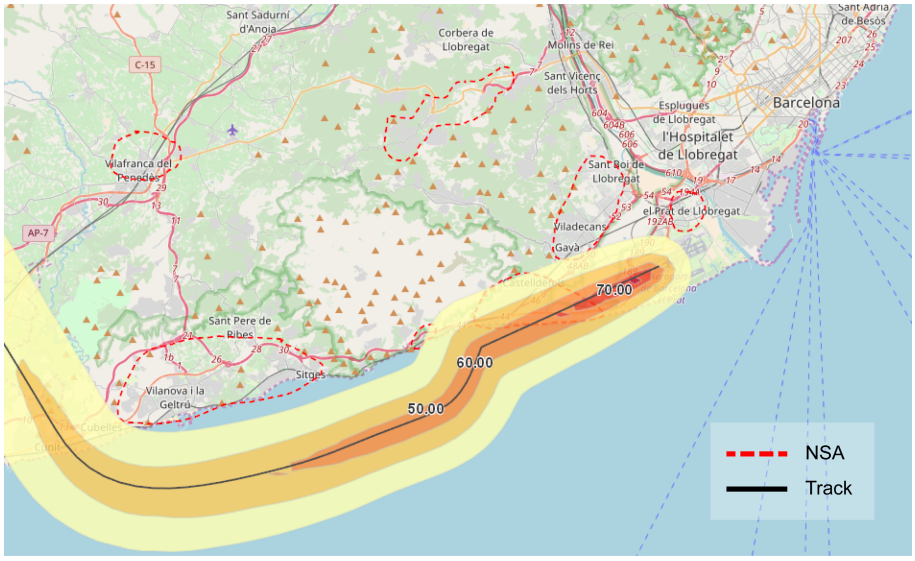

(b) h_{ILS} = 2000 ft

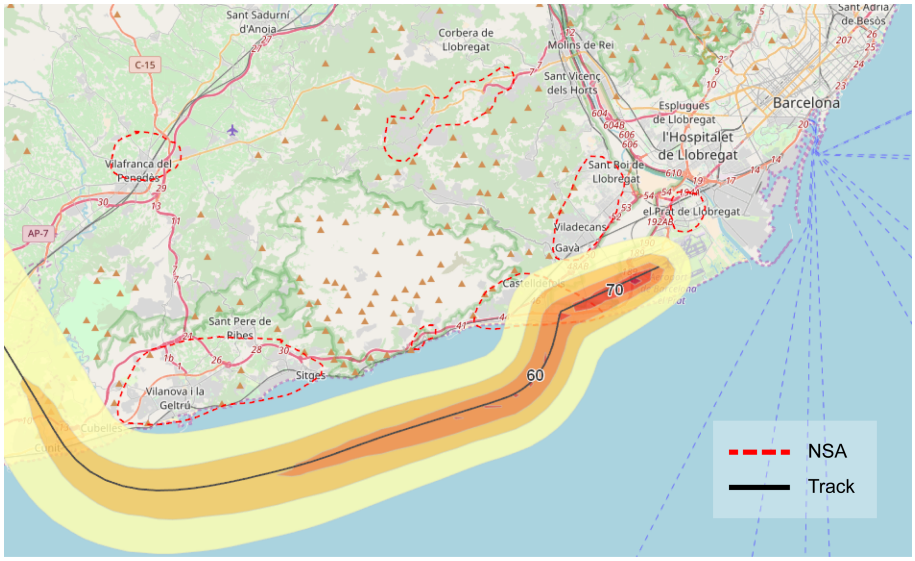

(c) h_{ILS} = 1000 ft

Figure 4.8: Case 1 noise footprints

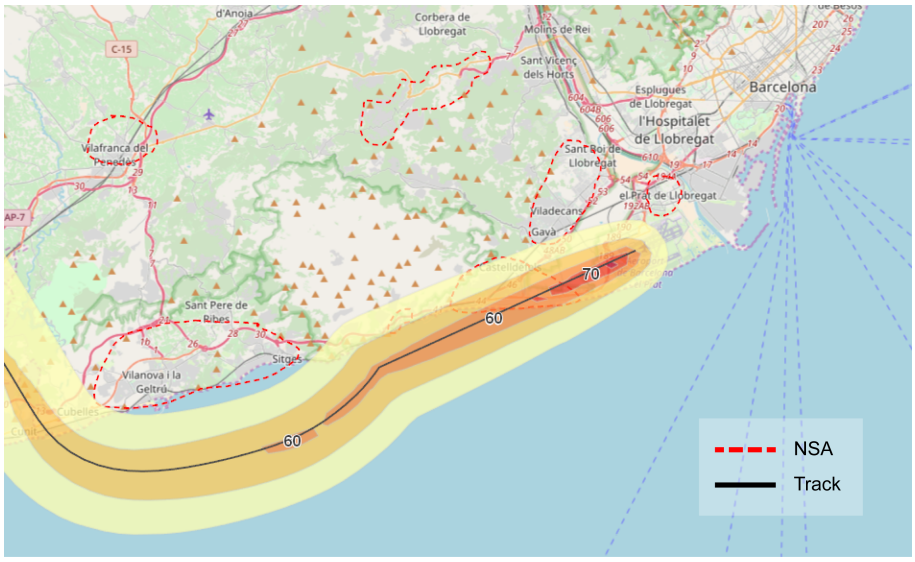

(a) h_{ILS} = 3000 ft

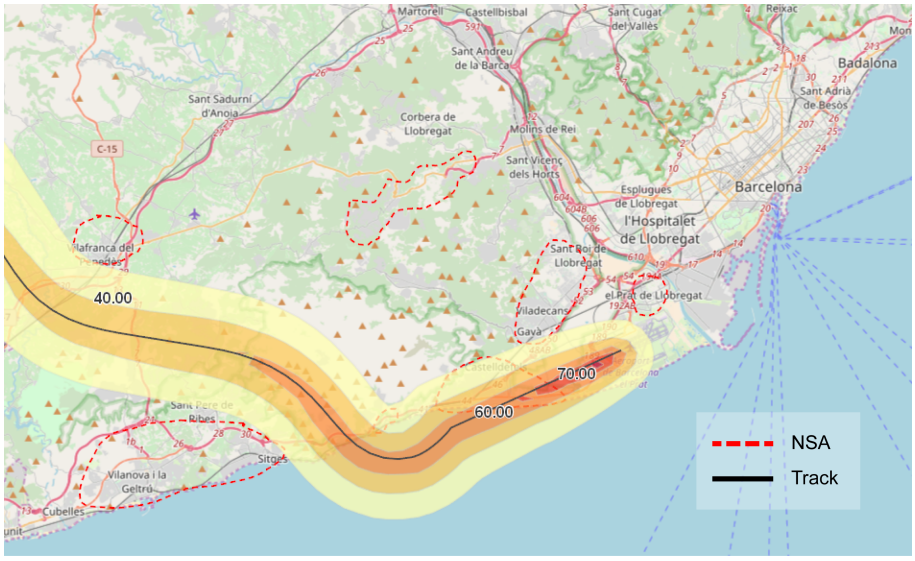

(b) h_{ILS} = 2000 ft

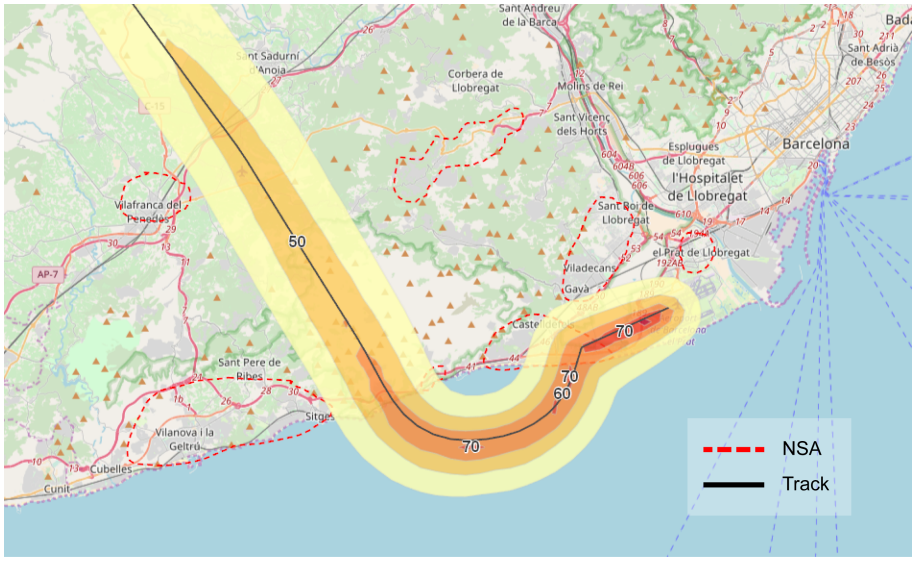

(c) h_{ILS} = 1000 ft

Figure 4.9: Case 2 noise footprints

CONCLUSIONS

From all the different results obtained throughout the project, which have been exposed in this document, several conclusions can be drawn.

As a starting point, this project brings together three main contributions. In the first place, the Noise-Power-Distance (NPD) tables used for computing noise levels at a given location, have been extrapolated to the desired operational boundaries and, in addition, have been approximated successfully as continuous and differentiable functions by means of splines. Secondly, a new method for measuring the noise impact over predefined noise sensitive areas has been defined. In this context, state-of-the-art methods based on discrete measuring points have been replaced by continuous surfaces, again, defined by splines functions. Last but not least, as a consequence of the newly implemented method for measuring the noise impact produced by aircraft trajectories, a new way of quantifying such an impact has been defined. Giving a unique noise level for every instant of time and, as a consequence, providing a better understanding of noise abatement procedures.

As a proof of concept, the arrival route for the Barcelona-El Prat airport (runway 07L), has been assessed, implementing a simple representation of the different Noise sensitive Areas (NSAs) surrounding the airport. The obtained results show how the trajectories meet the imposed requirements regarding Air Traffic Management (ATM) systems constraints and the correct functioning of the introduced methodology, which could be used as a tool to help regulators design new Noise Abatement Procedures (NAPs).

All this being said, to conclude, some more guidance on work which needs to be beard in mind in the future will be given. First, as mentioned above, although the exposed scenario has proven the proper function of the presented methodology, the solutions obtained are quite straightforward, as half of the scenario is covered by the sea. For this reason, in order to obtain more interesting solutions, a more complex scenario, based in an airport surrounded by NSAs, must be tested. Secondly, a new cost objective minimizing the noise impact over the worst affected zones must be better defined, with the aim of providing more equity to the obtained solution. In third place, it is important to implement NSAs where the elevation of the terrain is considered. Fourthly, as airframe noise is one of the main contributions to aircraft noise emissions, it would be useful to implement a noise model, where the position of the landing gear and aerodynamic configuration of the aircraft is considered. Fifth, it is important to assess the differences between the obtained trajectories and realistic scenarios currently being implemented in ATM systems. Last but not least, in order to properly verify the obtained results, it is required to check the obtained trajectories noise impact with an external noise model.

BIBLIOGRAPHY

[1] E. C. Kerrigan and J. M. Maciejowski. Designing model predictive controllers with prioritised constraints and objectives. In: *2002 IEEE International Symposium on Computer Aided Control System Design, CACSD 2002 - Proceedings*. 2002, 33–38. ISBN: 078037388X. DOI: 10.1109/CACSD.2002.1036925.

[2] H. G. Visser and R. a. A. Wijnen. Optimization of Noise Abatement Departure Trajectories. *Journal of Aircraft*, 38(4):620–627, 2001. ISSN: 0021-8669. DOI: 10.2514/2.2838.

[3] H. G. Visser and R. A. A. Wijnen. Optimisation of noise abatement arrival trajectories. *Aeronautical Journal*, 107(1076):607–615, 2003. ISSN: 00019240. DOI: 10.2514/2.2838.

[4] R. A. A. Wijnen and H. G. Visser. Optimal departure trajectories with respect to sleep disturbance. *Aerospace Science and Technology*, 7(1):81–91, 2003. ISSN: 12709638. DOI: 10.1016/S1270-9638(02)01183-5.

[5] X. Prats. Contributions to the Optimisation of Aircraft Noise Abatement Procedures. PhD thesis. 2010, 193.

[6] R. Dalmau, M. Melgosa, S. Vilardaga, and X. Prats. A Fast and Flexible Trajectory Predictor and Optimiser for ATM Research Applications. In: *7th International Conference on Research in Air Transportation (ICRAT)*. Castelldefels, Spain, 2018.

[7] ECAC. ECAC . CEAC Doc 29 3rd Edition Report on Standard Method of Computing Noise Contours around Civil Airports Volume 1 : Applications Guide, 2005.

[8] M. Arntzen and D. G. Simons. Modeling and synthesis of aircraft flyover noise. *Applied Acoustics*, 84:99–106, 2014. ISSN: 1872910X. DOI: 10.1016/j.apacoust.2013.09.002.

[9] ISO 226. *Acoustique – Lignes isosoniques normales*. 2003.

[10] D. Casalino, F. Diozzi, R. Sannino, and A. Paonessa. Aircraft noise reduction technologies: A bibliographic review. *Aerospace Science and Technology*, 12(1):1–17, 2008. ISSN: 12709638. DOI: 10.1016/j.ast.2007.10.004.

[11] F. Netjasov. Contemporary measures for noise reduction in airport surroundings. *Applied Acoustics*, 73(10):1076–1085, 2012. ISSN: 0003682X. DOI: 10.1016/j.apacoust.2012.03.010.

[12] International Civil Aviation Organization. Aircraft Operations. Volume I - Flight Procedures. *International Civil Aviation Organization*, I, 2006. ISSN: 0740722X.

[13] X. Prats, B. Bendris, R. Dalmau, J. Montolio, B. Day, H. Lenz, and R. Kohrs. 4D continuous descent operations supported by an electronic flight bag: A human-in-the-loop study. *AIAA/IEEE Digital Avionics Systems Conference - Proceedings*, 2016. ISSN: 21557209. DOI: 10.1109/DASC.2016.7778022.

[14] R. Dalmau, X. Prats, R. Verhoeven, F. Bussink, and B. Heesbeen. Performance comparison of guidance strategies to accomplish RTAs during a CDO. In: *AIAA/IEEE Digital Avionics Systems Conference - Proceedings*. Vol. 2017-Septe. 2017. ISBN: 9781538603659. DOI: 10.1109/DASC.2017.8102096.

[15] R. Dalmau and X. Prats. Controlled time of arrival windows for already initiated energy-neutral continuous descent operations. *Transportation Research Part C: Emerging Technologies*, 85:334–347, 2017. ISSN: 0968090X. DOI: 10.1016/j.trc.2017.09.024.

[16] R. Dalmau and X. Prats. Fuel and time savings by flying continuous cruise climbs. Estimating the benefit pools for maximum range operations. *Transportation Research Part D: Transport and Environment*, 35:62–71, 2015. ISSN: 13619209. DOI: 10.1016/j.trd.2014.11.019.

[17] R. Verhoeven, R. Dalmau, X. Prats, and N. De Gelder. Real-time aircraft continuous descent trajectory optimization with ATC time constraints using direct collocation methods. In: *29th Congress of the International Council of the Aeronautical Sciences (ICAS) - Proceedings*. 2014. ISBN: 3932182804.

[18] S. Ramasamy, R. Sabatini, M. Marino, A. Gardi, and T. Kistan. Aircraft Noise Modelling and 4D Trajectory Optimisation Methods for Reduced Environmental Impacts at Airports. *International Symposium on Sustainable Aviation - Proceedings*, 2015. DOI: 10.13140/RG.2.1.1425.4245.

[19] A. Gardi, R. Sabatini, and S. Ramasamy. Multi-objective optimisation of aircraft flight trajectories in the ATM and avionics context. *Progress in Aerospace Sciences*, 83:1–36, 2016. ISSN: 03760421. DOI: 10.1016/j.paerosci.2015.11.006.

[20] ECAC. *ECAC . CEAC Doc 29 3rd Edition Report on Standard Method of Computing Noise Contours around Civil Airports Volume 2 : Technical Guide*. Tech. rep. 2005.

[21] X. Prats, V. Puig, and J. Quevedo. Equitable Aircraft Noise-Abatement Departure Procedures. *Journal of Guidance, Control, and Dynamics*, 34(1):192–203, 2011. ISSN: 0731-5090. DOI: 10.2514/1.49530.

[22] X. Prats, V. Puig, J. Quevedo, and F. Nejjari. Equitable noise abatement departure procedures. *9th AIAA Aviation Technology, Integration, and Operations Conference - Proceedings*, (September):1–11, 2009.

[23] M. Zhang, A. Filippone, and N. Bojdo. Using Trajectory Optimization to Minimize Aircraft Noise Impact. *Inter Noise - Proceedings, 27-30 August 2017, Hong Kong*.

[24] A. E. Bryson, Y.-C. Ho, and G. M. Siouris. Applied Optimal Control: Optimization, Estimation, and Control. *IEEE Transactions on Systems, Man, and Cybernetics*, 9(6):366–367, 1979. ISSN: 0018-9472. DOI: 10.1109/TSMC.1979.4310229.

[25] N. Shinohara, K. Hanaka, and I. Yamada. Study of lateral attenuation under meteorological conditions for airport noise modeling:795–804, 2016. ISSN: 0001-4966. DOI: 10.1121/1.4970307.

[26] Eurocontrol Experimental Centre (Eurocontrol). *Concept Document for the Base of Aircraft Data (BADA) Family 4*. Tech. rep. 2000. DOI: 10.1177/1090820X10391211.

[27] J. R. and C. de Boor. A Practical Guide to Splines. *Mathematics of Computation*, 34(149):325, 1980. ISSN: 00255718. DOI: 10.2307/2006241. arXiv: 1501.02634.

[28] X. Prats, S. Vilardaga, R. Isanta, I. Bas, and F. Birling. WEMSgen: A real-time weather modelling library for on-board trajectory optimisation and planning. *AIAA/IEEE Digital Avionics Systems Conference - Proceedings*:6A11–6A115, 2015. ISSN: 21557209. DOI: 10.1109/DASC.2015.7311441.

[29] P. Dierckx. *Curve and Surface Fitting with Splines*. New York, NY, USA: Oxford University Press, Inc., 1993. ISBN: 0-19-853441-8.